Unimolecular thermal fragmentation of *ortho*-benzyne

Xu Zhang[a] and Alan T. Maccarone[b]
Department of Chemistry and Biochemistry, University of Colorado, Boulder, Colorado 80309-0215

Mark R. Nimlos[c]
National Renewable Energy Laboratory, 1617 Cole Boulevard, Golden, Colorado 80401

Shuji Kato,[d] Veronica M. Bierbaum,[e] and G. Barney Ellison[f]
Department of Chemistry and Biochemistry, University of Colorado, Boulder, Colorado 80309-0215

Branko Ruscic[g]
Chemistry Division, Argonne National Laboratory, 9700 South Cass Avenue, Argonne, Illinois 60439

Andrew C. Simmonett,[h] Wesley D. Allen,[i] and Henry F. Schaefer III[j]
Center for Computational Chemistry, University of Georgia, Athens, Georgia 30602 and Department of Chemistry, University of Georgia, Athens, Georgia 30602

(Received 11 August 2006; accepted 20 November 2006; published online 26 January 2007)

The *ortho*-benzyne diradical, *o*-C_6H_4 has been produced with a supersonic nozzle and its subsequent thermal decomposition has been studied. As the temperature of the nozzle is increased, the benzyne molecule fragments: *o*-$C_6H_4+\Delta\rightarrow$ products. The thermal dissociation products were identified by three experimental methods: (i) time-of-flight photoionization mass spectrometry, (ii) matrix-isolation Fourier transform infrared absorption spectroscopy, and (iii) chemical ionization mass spectrometry. At the threshold dissociation temperature, *o*-benzyne cleanly decomposes into acetylene and diacetylene via an apparent retro-Diels-Alder process: *o*-$C_6H_4+\Delta\rightarrow HC{\equiv}CH+HC{\equiv}C-C{\equiv}CH$. The experimental $\Delta_{rxn}H_{298}$(*o*-$C_6H_4\rightarrow HC{\equiv}CH+HC{\equiv}C-C{\equiv}CH$) is found to be 57 ± 3 kcal mol^{-1}. Further experiments with the substituted benzyne, 3,6-$(CH_3)_2$-*o*-C_6H_2, are consistent with a retro-Diels-Alder fragmentation. But at higher nozzle temperatures, the cracking pattern becomes more complicated. To interpret these experiments, the retro-Diels-Alder fragmentation of *o*-benzyne has been investigated by rigorous *ab initio* electronic structure computations. These calculations used basis sets as large as [C(7*s*6*p*5*d*4*f*3*g*2*h*1*i*)/H(6*s*5*p*4*d*3*f*2*g*1*h*)] (cc-pV6Z) and electron correlation treatments as extensive as full coupled cluster through triple excitations (CCSDT), in cases with a perturbative term for connected quadruples [CCSDT(Q)]. Focal point extrapolations of the computational data yield a 0 K barrier for the concerted, C_{2v}-symmetric decomposition of *o*-benzyne, E_b(*o*-$C_6H_4\rightarrow HC{\equiv}CH+HC{\equiv}C-C{\equiv}CH)=88.0\pm0.5$ kcal mol^{-1}. A barrier of this magnitude is consistent with the experimental results. A careful assessment of the thermochemistry for the high temperature fragmentation of benzene is presented: $C_6H_6\rightarrow H+[C_6H_5]\rightarrow H+[o\text{-}C_6H_4]\rightarrow HC{\equiv}CH+HC{\equiv}C-C{\equiv}CH$. Benzyne may be an important intermediate in the thermal decomposition of many alkylbenzenes (arenes). High engine temperatures above 1500 K may crack these alkylbenzenes to a mixture of alkyl radicals and phenyl radicals. The phenyl radicals will then dissociate first to benzyne and then to acetylene and diacetylene. © *2007 American Institute of Physics*. [DOI: 10.1063/1.2409927]

I. INTRODUCTION

This is a combined experimental and theoretical study of the thermal fragmentation of benzyne. We have used a high temperature nozzle to observe the thermal fragmentation of benzyne (a C_6H_6 fragmentation product) to acetylene and diacetylene. The analysis of the pyrolysis products emerging from the hyperthermal nozzle is based on three analytical techniques: (i) time-of-flight photoionization mass spectrometry (TOF-PIMS), (ii) matrix-isolation Fourier transform infrared absorption spectroscopy (matrix-isolation FTIR), and (iii) chemical ionization mass spectrometry (CIMS). To better interpret these experiments we have used high-level *ab initio* electronic structure computations [fully optimized structures and corresponding vibrational frequencies at the valence CCSD(T)/cc-pVTZ and composite all-electron CCSD(T)/cc-pCVQZ levels of theory with focal point extrapolations of the energetics to the complete basis set (CBS) CCSDT(Q) limit] to characterize the transition state for the

[a]Electronic mail: xu.zhang@colorado.edu
[b]Electronic mail: alan.maccarone@colorado.edu
[c]Electronic mail: mark_nimlos@nrel.gov
[d]Electronic mail:shuji.kato@colorado.edu
[e]Electronic mail:veronica.bierbaum@colorado.edu
[f]Electronic mail:barney@jila.colorado.edu
[g]Electronic mail:ruscic@anl.gov
[h]Electronic mail: andysim@ccc.uga.edu
[i]Electronic mail:wdallen@ccqc.uga.edu
[j]Electronic mail: hfs@uga.edu

 © 2007 American Institute of Physics

C_{2v} symmetric, retro-Diels-Alder fragmentation: $[o\text{-}C_6H_4]^{\ddagger} \rightarrow HC{\equiv}CH + HC{\equiv}C{-}C{\equiv}CH$. Finally, an analysis of thermochemistry of toluene and more complex arenes is presented. The high temperature thermochemistry of these arenes suggests that one might generalize the retro-Diels-Alder mechanism for benzene dissociation [Eqs. (1)–(3)] to include the high temperature ($T > 1500$ K) fragmentation of many alkyl benzenes.

The thermal fragmentation of benzene has been extensively studied in shock tubes[1,2] and theoretically.[3–6] Most mechanisms have the C–H bond fission as the first step[2] to produce H atom and the phenyl radical,

$$C_6H_6 + M \rightarrow C_6H_5 + H + M. \quad (1)$$

As noted by Kiefer *et al.*,[2] benzene decomposition at modest temperatures yields equal amounts of HCCH and HCC–CCH as the dominant products. However, in all of these flow reactor, Knudsen cell, and shock tube studies there is a surprising absence of C_6H_5 signals.

The fate of the phenyl radical is of great interest[3–6] and much evidence suggests that the phenyl radicals further eliminate a second H atom to produce the 1,2-diradical *ortho*-benzyne ($o\text{-}C_6H_4$).

$$C_6H_5 + M \rightarrow o\text{-}C_6H_4 + H + M. \quad (2)$$

A possible fate of $o\text{-}C_6H_4$ is fragmentation to acetylene and diacetylene,

$$o\text{-}C_6H_4 + \Delta \rightarrow HC{\equiv}CH + HC{\equiv}C{-}C{\equiv}CH. \quad (3)$$

We should consider several different dissociation pathways for *o*-benzyne. Path A is a concerted, C_{2v} symmetric bond rupture of $o\text{-}C_6H_4$ and is a retro-Diels-Alder reaction. A concerted reaction implies that there are no bound intermediates between $o\text{-}C_6H_4$ and the acetylene/diacetylene fragments. Path B is a concerted asymmetric bond rupture of the $o\text{-}C_6H_4$ diradical. Or a final possibility is Path C, a nonconcerted, asymmetric bond rupture of the $o\text{-}C_6H_4$ diradical to produce an open-chain diradical intermediate. Subsequent decomposition of this diradical intermediate produces acetylene/diacetylene:

$$[o\text{-}C_6H_4]^{\ddagger} \rightarrow [HC{=}\ddot{C}{-}\dddot{C}{=}CH{-}CH{=}CH\cdot] \rightarrow HC{\equiv}CH + HC{\equiv}C{-}C{\equiv}CH.$$

There also exists the possibility that $o\text{-}C_6H_4$ may isomerize before it fragments. Instead of dissociating via Eq. (3), $o\text{-}C_6H_4$ could rearrange first to *m*-benzyne and then to *p*-benzyne. At 1000 K it has been predicted that $o\text{-}C_6H_4$ overwhelmingly isomerizes to *p*-benzyne, which could undergo[5] a Bergman fragmentation[7,8] to the enediyne, (Z)–HCC–CH=CH–CCH at higher temperatures. Scheme I shows these related reactions.

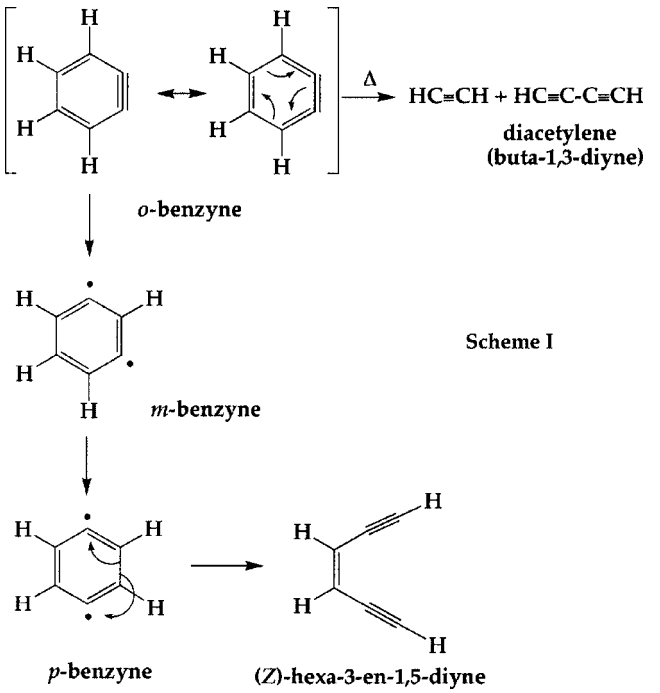

Scheme I

In order to understand Eqs. (1)–(3), it is essential to have a firm grasp of the thermochemistry. We need accurate values for the following heats of formation: $\Delta_f H_{298}(C_6H_6)$, $\Delta_f H_{298}(C_6H_5)$, $\Delta_f H_{298}(o\text{-}C_6H_4)$, $\Delta_f H_{298}(m\text{-}C_6H_4)$, $\Delta_f H_{298}(p\text{-}C_6H_4)$, $\Delta_f H_{298}$(HCC–CH=CH–CCH), $\Delta_f H_{298}$(HCCH), and $\Delta_f H_{298}$(HCC–CCH). For the energies of closed-shell species such as benzene and acetylene, we have used standard tables.[9] But the thermochemistry of phenyl radical, the benzynes, diacetylene, and the enediyne, (Z)–HCC–CH=CH–CCH, is not routinely tabulated.

In an experimental study[10] of the high temperature pyrolysis of acetylene, the heat of formation of diacetylene (HC≡C–C≡CH, buta-1,3-diyne) was quoted as $\Delta_f H_{298}$(HCC–CCH) = 111 kcal mol^{-1}. This paper used results from an earlier set of group additivity estimates[11] which placed $\Delta_f H_{298}$(HCC–CCH) in the range between 105 and 113 kcal mol^{-1}. There seems to be no reliable experimental thermochemistry for diacetylene, so we have used electronic structure computations to pinpoint $\Delta_f H_{298}$(diacetylene) by means of the isogyric reaction HC≡C–C≡CH + $H_2 \rightarrow$ 2 HCCH. Focal-point extrapolations conjoining MP2/cc-pV6Z, CCSD(T)/cc-pV5Z, and CCSDT(Q)/cc-pVDZ results (*vide infra*) yield $\Delta_f H_{298}$(diacetylene) = 109.4 ± 0.3 kcal mol^{-1}.

Calometric studies of the catalytic hydrogenation of the enediyne have been carried out and it is reported[12] that the solution heat of formation is $\Delta_f H_{298}$[(Z)–HCC–CH=CH–CCH] = 129.5 kcal mol^{-1}. Most of the thermochemistry for the remaining aryl radicals and diradicals is available via the negative ion/acidity thermochemical cycle.[13,14]

The phenyl radical, C_6H_5, is known by electron paramagnetic resonance studies[15] and infrared absorption studies[16,17] to be a C_{2v} species with a $\tilde{X}\,^2A_1$ ground state. The microwave spectrum of the C_6H_5 radical has been detected,[18] but as yet the molecular structure has not been determined.

Photoionization studies[19] of phenyl have reported $IE(C_6H_5)=8.32\pm0.04$ eV; however, more recent photoelectron spectroscopic studies[20] of beams of the phenyl radical find a slightly lower value: $IE(C_6H_5)=8.1\pm0.1$ eV. Negative ion photodetachment studies[21] established the electron affinity of the phenyl radical, $EA(C_6H_5)$, to be 1.096 ± 0.006 eV. The use of the gas-phase enthalpy of deprotonation of benzene,[22,23] $\Delta_{acid}H_{298}(C_6H_5-H)=401.2\pm0.2$ kcal mol^{-1}, and the $EA(C_6H_5)$ in the acidity/EA thermochemical cycle[13,14] furnished the bond energy of benzene, $DH_{298}(C_6H_5-H)=112.9\pm0.5$ kcal mol^{-1}. Since the heat of formation of benzene is known[9] to be $\Delta_fH_{298}(C_6H_6)=19.7\pm0.2$ kcal mol^{-1}, the value of the C–H bond energy determines the heat of formation of the phenyl radical to be $\Delta_fH_{298}(C_6H_5)=80.5\pm0.5$ kcal mol^{-1}.

Almost 50 years ago, a series of pioneering papers[24–26] clearly demonstrated that samples of gaseous benzyne could be generated. Rudimentary UV absorption spectra and EI mass spectra were reported[26–28] for all isomers of C_6H_4. The *o*-benzyne diradical, 1,2-dehydrobenzene, has been detected by microwave spectroscopy[29] and analyzed[30,31] to be a planar, C_{2v} ring. The ground state of *o*-C_6H_4 is $\tilde{X}\,^1A_1$. The ionization potential of this diradical was measured[32] to be $IE(o\text{-}C_6H_4)=9.03\pm0.05$ eV. The ground state of the benzyne cation (o-$C_6H_4^+$) was assigned to be a "π-cation," $\tilde{X}\,^2A_2$ and there is surely a second, nearly degenerate π-cation state, $\tilde{A}\,^2B_1$. The term value of the excited "σ-cation" state was found to be $T_0(\tilde{B}\,^2A_1-\tilde{X}\,^2A_2)=0.74\pm0.06$ eV.

The two lowest electronic states of *o*-C_6H_4 can be represented[33] by a pair of electrons in the lobe orbitals $\{\ell_a,\ell_b\}$ that are coupled singlet ($^1A_1$) or triplet ($^3B_2$).

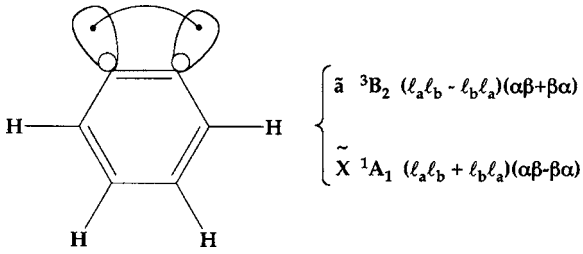

(4)

Negative ion beams of the $C_6H_4^-$ anion were photodetached[34] and the electron affinity was measured to be $EA(o\text{-}C_6H_4)=0.560\pm0.010$ eV. Negative ion photoelectron spectroscopy established the intercombination gap, $T_0(\tilde{a}\,^3B_2-\tilde{X}\,^1A_1)=1.637\pm0.025$ eV as well as the value of the vibrational frequency of the CC "triple bond," $\nu_3(o\text{-}C_6H_4)=1860\pm15$ cm^{-1}. Subsequent infrared studies[35] in a Ne matrix confirm the assignment of the weak band, $\nu_3(o\text{-}C_6H_4)$, to be 1846 cm^{-1}.

If the gas-phase acidity of the phenyl radical could be measured, the acidity/EA thermochemical cycle[13] could be applied to extract the C–H bond energy of the phenyl radical: $\Delta_{acid}H_{298}(C_6H_5)=DH_{298}(C_6H_4\text{-}ortho\text{-}H)+IE(H)-EA(o\text{-}C_6H_4)$. Measurement of the acidity of a radical such as C_6H_5 is not straightforward. Early flowing afterglow proton transfer studies[36] of the *o*-$C_6H_4^-$ anion were only able to bracket the acidity of the phenyl radical; $\Delta_{acid}H_{298}(C_6H_5)=379^{+6}_{-3}$ kcal mol^{-1}. With this approximate acidity, the C–H bond energy of the phenyl radical α to the radical site becomes $DH_{298}(C_6H_4\text{-}ortho\text{-}H)=78\pm6$ kcal mol^{-1} and $\Delta_fH_{298}(o\text{-}C_6H_4)=107\pm6$ kcal mol^{-1}.

The heat of formation of *o*-benzyne was improved by a FT-ICR study[37] of the energetics of the dehalogenation reaction: $OH^-+C_6H_5I\rightarrow(H_2O\cdot I)^-+o\text{-}C_6H_4$. By estimating the stability of the clustered halide ion, $(H_2O\cdot I)^-$, this study concluded that $\Delta_fH_{298}(o\text{-}C_6H_4)=105\pm2$ kcal mol^{-1} and $DH_{298}(C_6H_4\text{-}ortho\text{-}H)=77\pm2$ kcal mol^{-1}. Finally, collision-induced threshold dissociation studies of deprotonated chlorobenzene[38] provided another independent route [Eq. (5)] to establish the heat of formation of *o*-benzyne.

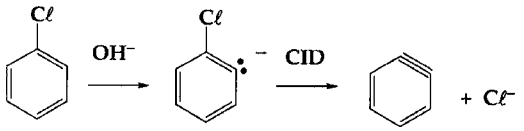

(5)

These threshold dissociation studies reported $\Delta_fH_{298}(o\text{-}C_6H_4)=107\pm3$ kcal mol^{-1} and $DH_{298}(C_6H_4\text{-}ortho\text{-}H)=78\pm3$ kcal mol^{-1}. Parallel studies of the *meta*- and *para*-chlorophenide anions could be analyzed[39] to find the other C–H bond energies of the phenyl radical: $DH_{298}(C_6H_4\text{-}meta\text{-}H)=94\pm3$ kcal mol^{-1} and $DH_{298}(C_6H_4\text{-}para\text{-}H)=109\pm3$ kcal mol^{-1}. These experimental benzene and benzyne bond energies[9,14] are summarized in Scheme II.

Scheme II

Arene Bond Dissociation Enthalpies, DH_{298}, kcal mol^{-1}

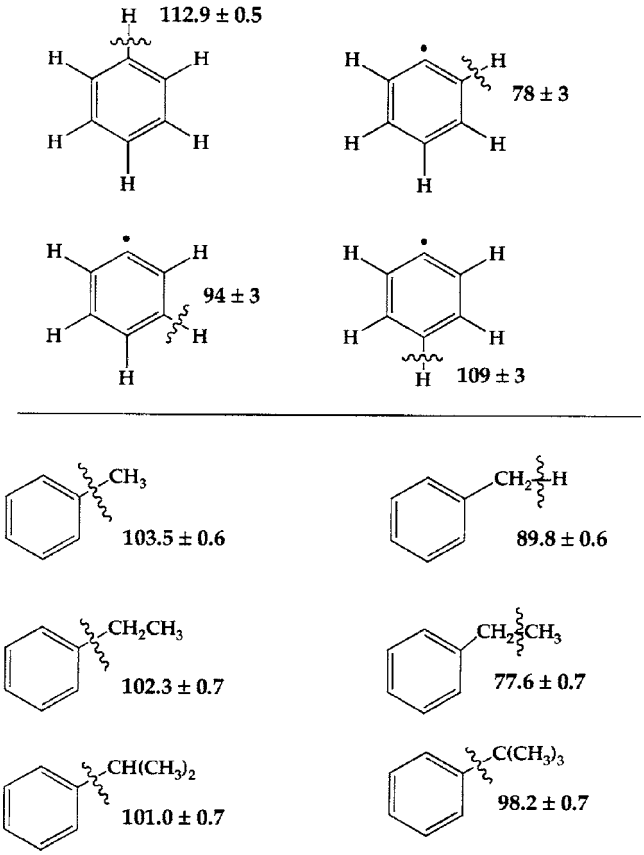

II. EXPERIMENTAL METHODS

Molecular beams of *o*-benzyne and 3,6-dimethyl-*o*-benzyne were prepared in a hyperthermal nozzle that has been described previously.[40] To simplify the discussion in this paper, the nozzle temperature will be categorized as *room temperature, low heat, medium heat*, and *high heat*, instead of the specific temperature (in K or °C) used previously.[41] In general, the following temperature ranges apply to these heating categories: room temperature implies 300 K, low heat implies 1200–1400 K, medium heat implies 1400–1600 K, and high heat implies 1600–1800 K.

Benzoyl chloride ($C_6H_5COC\ell$) is a convenient source of *o*-benzyne.

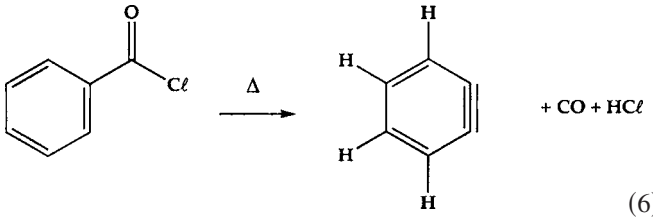

(6)

The reaction enthalpy[9,14] is measured to be $\Delta_{rxn}H_{298}(6) = 83 \pm 3$ kcal mol^{-1}. In addition to benzoyl chloride, 1,2-diiodobenzene ($C_6H_4I_2$) is an effective *o*-benzyne precursor.

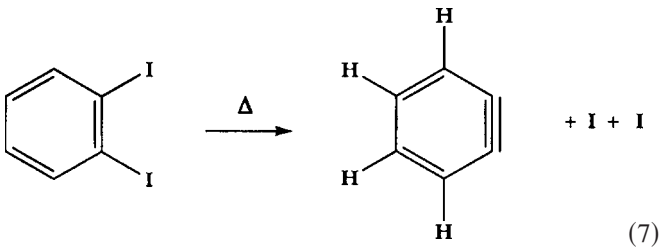

(7)

Diiodobenzene probably decomposes by sequential cracking of the C–I bonds since the bond energy of iodobenzene is only $DH_{298}(C_6H_5-I) = 67 \pm 2$ kcal mol^{-1}. The enthalpy[9,14] is measured to be $\Delta_{rxn}H_{298}(7) = 97 \pm 3$ kcal mol^{-1}.

The diketone, benzocyclobutene-1,2-dione [$C_6H_4(CO)_2$], is an elegant source[20,42] of *o*-benzyne. The thermochemistry of Eq. (8) is unknown.

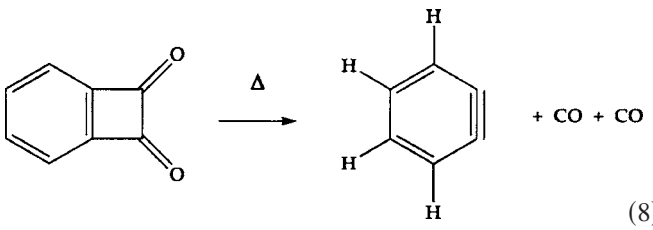

(8)

Bromobenzene (C_6H_5Br) was used to generate the phenyl radical (C_6H_5), which further fragments to *o*-benzyne.

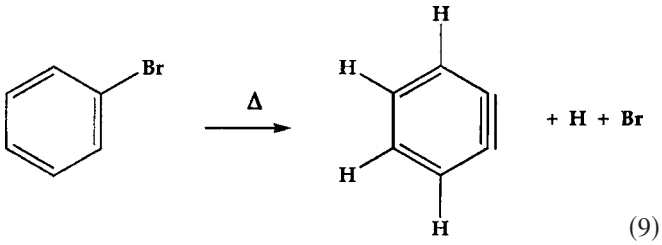

(9)

Bromobenzene fragments by rupture of the C–Br bond [$DH_{298}(C_6H_5-Br) = 82 \pm 1$ kcal mol^{-1}] followed by H expulsion from the phenyl radical (see Scheme II). The enthalpy[9,14] is $\Delta_{rxn}H_{298}(9) = 160 \pm 3$ kcal mol^{-1}.

Finally, we have used 2,5-dimethylbenzoyl chloride, $(CH_3)_2C_6H_3COC\ell$, as an *o*-benzyne precursor [Eq. (10)] to study the regiochemistry of benzyne cracking.

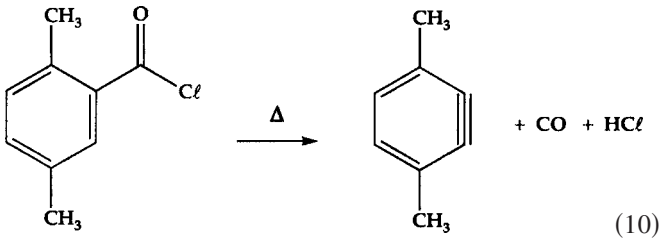

(10)

All precursors were purchased from Sigma-Aldrich, with the exception of benzocyclobutene-1,2-dione and 2,5-dimethylbenzoyl chloride, which were purchased from Molecular Diversity Preservation International and Advanced Synthesis Technologies, respectively. All compounds had a purity of 95% or higher and were used as prepared by their respective companies.

To identify the pyrolysis products emerging from the hyperthermal nozzle, we have employed three analytical techniques: (i) time-of-flight photoionization mass spectrometry, (ii) matrix-isolation Fourier transform infrared absorption spectroscopy, and (iii) chemical ionization mass spectrometry. Each will be briefly described below.

(i) TOF-PIMS. The photoionization mass spectrometer we have employed is housed at the DOE's National Renewable Energy Laboratory in Golden, CO. A description of this instrument has been previously reported.[40,43] In brief, the ninth harmonic of a Nd:YAG (yttrium aluminum garnet) laser (Continuum PL8010) at $\lambda = 118.2$ nm is generated by frequency tripling the 355 nm output (10 Hz, 40 mJ/pulse) from the laser in a xenon cell (roughly 4 Torr Xe mixed with 40 Torr Ar). After exiting the tripling cell, the vacuum ultraviolet photons cross a molecular beam of organic radicals. Most organics have ionization energies less than 10 eV and will be photoionized by the 10.487 eV laser photon. The photoions travel through a reflectron time-of-flight mass spectrometer (R.M. Jordan Co.), where the signal is detected and sent to a computer for collection.

The supersonic molecular beam of organic radicals is generated in a supersonic hyperthermal nozzle.[40] A SiC tube (2.5 cm length, 1 mm ID, 2 mm OD) sits on top of a solenoid pulsed valve (Parker Hannifin Corp.) and is resistively heated. In one configuration, a gas mixture of 0.1% precursor in helium (roughly 2 atm total pressure) is prepared in a

manifold that is connected to the valve; this works for relatively volatile precursors. In another configuration, for nonvolatile precursors such as those used in this study, the precursor is placed in a glass tube (2.5 cm length, 1 mm ID, 2 mm OD) that is put behind the body of the valve. The valve is wrapped with nichrome wire for resistive heating to increase the vapor pressure of the precursor. Helium is passed over the heated sample to carry the vapor through the valve and into the SiC tube, where it undergoes thermal decomposition. The product radicals reside in the SiC tube for roughly 30 μs. This short residence time dramatically reduces side reactions and increases radical yield. After exiting the SiC tube, the radicals supersonically expand into a region near 5×10^{-6} Torr and the beam is skimmed on its way into the laser photoionization region. Photoions are extracted into the time-of-flight tube, which is mutually orthogonal to the radical beam and the laser beam.

(ii) Matrix-isolation FTIR. Matrix-isolation FTIR is used to study the vibrational spectrum of organic radicals generated in the supersonic, hyperthermal nozzle.[40,44] The experimental components involved in the matrix studies are very similar to those used in the TOF-PIMS experiments except for the use of argon instead of helium as the carrier gas. After supersonically expanding from the nozzle into a region on the order of 5×10^{-5} Torr, the radical/argon beam travels about 25 mm (25 nozzle ID) where it is deposited onto a CsI window (2.5 cm diameter, 5 mm thick) at 15 K. The CsI window is cooled by a helium cryostat (APD Cryogenics Inc.). The argon atoms surround the radicals, forming a matrix that prevents the radicals from undergoing further reactions. After deposition over a period of several hours, the matrix is analyzed using a FTIR spectrometer (Nicolet Magna 550) interfaced to a computer for signal processing. The spectra are recorded with either a MCT-A ($8000-550$ cm^{-1}) or a MCT-B ($5000-400$ cm^{-1}) detector.

(iii) Chemical ionization mass spectrometry. The CIMS experiments were carried out in a flowing afterglow selected ion flow tube (FA-SIFT) instrument coupled with the supersonic hyperthermal nozzle.[45,46] The reagent ions, H_3O^+ or HO^-, are generated in the source flow tube by electron ionization and ion-molecule reactions. The ions are then mass selected with the SIFT quadrupole mass filter and injected into the reaction flow tube (7.3 cm ID and roughly 1 m long) containing a helium buffer gas (0.5 Torr, 300 K) flowing at a velocity of about 95 m s^{-1}. The SIFT injection produces a continuous flow of ions (approximately 10^5 particles cm^{-3}) in a stream of helium. The radical source is mounted to the flow tube after the SIFT quadrupole mass filter. Streams of *o*-C_6H_4 diradicals are generated through pyrolysis of $C_6H_5COC\ell$. Benzoyl chloride seeded in helium (roughly 0.5 Torr in 600 Torr) passes through a pulsed valve (20–40 Hz) into the resistively heated SiC nozzle. The pyrolysis products along with the He carrier gas expand supersonically through the nozzle into the flow tube. The gas transit time from the radical source to the detection sampling orifice is approximately 10 ms. The ionic species (both the reactant and products) are detected using the quadrupole mass spectrometer at the end of the flow tube.

III. ELECTRONIC STRUCTURE METHODS

The cc-pV*X*Z (*X*=D, T, Q, 5, 6) family of correlation-consistent, atomic-orbital basis sets[47–49] was employed in this study. The contracted Gaussian orbitals in these [C/H] sets extend from $[3s2p1d/2s1p]$ (DZ) to $[7s6p5d4f3g2h1i/6s5p4d3f2g1h]$ (6Z), the latter comprising 1204 functions for the C_6H_4 system. Core correlation effects were accounted for by all-electron (AE) computations with the cc-pCVTZ and cc-pCVQZ basis sets.[49,50] All polarization manifolds contained only pure spherical harmonics.

Reference electronic wave functions were primarily determined by the single-configuration, self-consistent-field, restricted Hartree-Fock (RHF) method,[51–54] but test computations were also performed with the complete-active-space self-consistent-field (CASSCF) approach.[55] The CASSCF procedures involved an active space of 12 electrons in 12 orbitals, selected by the criterion of lowest orbital energy. Dynamical electron correlation was accounted for by second-order Møller-Plesset perturbation theory (MP2),[54,56–58] by the coupled cluster singles and doubles method (CCSD),[57,59–64] and by CCSD theory augmented with either a perturbative[65,66] or full[67–69] inclusion of connected triple excitations. Final energetic determinations incorporated computations with the recently implemented CCSDT(Q) method[70] for the treatment of connected quadruple excitations. Unless otherwise stated, the carbon 1*s* core electrons were frozen in all correlation treatments.

Basis set extrapolations, an integral feature of the focal-point analysis method[71–75] for inferring *ab initio* limits, utilized the asymptotic formulas $E_x=E_{\mathrm{CBS}}+a\exp(-bX)$ and $\varepsilon_x=\varepsilon_{\mathrm{CBS}}+aX^{-3}$ for Hartree-Fock[76] and correlation energies,[77] respectively, where *X* is the cardinal number of the cc-pV*X*Z series and CBS denotes the complete basis set limit.

Geometric structures were optimized to at least 10^{-6} Å and 0.0001° using analytic gradient[78] techniques at the RHF, MP2, CCSD,[79] and CCSD(T)[80] levels of theory. Final structures were obtained by gradient-driven, full energy (*E*) minimizations of a composite approximation (c~) to CCSD(T)-AE/cc-pCVQZ,

$$\begin{aligned} E[c\sim\text{CCSD(T)-AE/cc-pCVQZ}] &\equiv E[\text{CCSD(T)/cc-pVTZ}] \\ &+ E[\text{MP2-AE/cc-pCVQZ}] \\ &- E[\text{MP2/cc-pVTZ}]. \end{aligned} \tag{11}$$

Quadratic force constants for harmonic vibrational frequency analyses were generally obtained via analytic second derivatives,[78,81–83] except in the CCSD(T)/cc-pVTZ case, where force fields were determined by numerical differentiation of analytic first derivatives,[84,85] and in selected c~CCSD(T)-AE/cc-pCVQZ benchmark runs, where energy points were used in careful double finite-difference procedures. Zero-point vibrational energies (ZPVEs) were computed from unscaled CCSD(T)/cc-pVTZ harmonic frequencies.

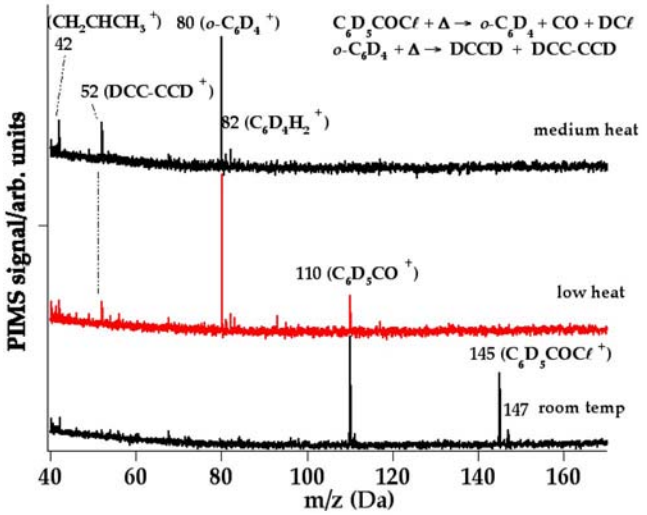

FIG. 1. TOF photoionization mass spectra from supersonic hyperthermal nozzle decomposition of benzoyl-d_5 chloride, with nozzle temperatures at room temperature, low heat, and medium heat. *o*-Benzyne-d_4 is detected at m/z 80 (o-$C_6D_4^+$). At room temperature, ions resulting from ionization of benzoyl-d_5 chloride are detected: m/z 145 and 147 ($C_6D_5COC\ell^+$) and m/z 110 ($C_6D_5CO^+$ from ionization-dissociation of $C_6D_5COC\ell$). At low heat, the precursor has largely decomposed to form *o*-benzyne shown at m/z 80 (o-$C_6D_4^+$). The signal at m/z 110 is attributed to residual precursor. The small peak at m/z 52 corresponds to ionized diacetylene $(DC{\equiv}C{-}C{\equiv}CD)^+$. At medium heat, the peak at m/z 52 increases, indicating more thermal cracking of *o*-benzyne. The small signal at m/z 82 might be benzene ($C_6D_4H_2^+$) which may result from secondary reactions of *o*-benzyne (o-C_6D_4). The signals from the precursor are absent, and the feature at m/z 42 belongs to an added mass marker, propene ($C_3H_6^+$).

All electronic structure computations were performed with either the Mainz-Austin-Budapest version of the ACESII package,[86] the MOLPRO suite,[87] NWCHEM,[88,89] or MRCC.[90]

IV. EXPERIMENTAL RESULTS

A. Detection and thermal decomposition of *o*-benzyne

1. TOF-PIMS of $C_6D_5COC\ell$

Earlier we used benzoyl chloride as a convenient source of *o*-benzyne.[45,46] Figure 1 illustrates the TOF-PIMS spectrum of the thermal decomposition of deuterated benzoyl chloride, $C_6D_5COC\ell$. It demonstrates the production of o-C_6D_4, which subsequently fragments to produce $DC{\equiv}CD$ and $DC{\equiv}C{-}C{\equiv}CD$. The bottom trace shows the background ions resulting from ionization of room temperature $C_6D_5COC\ell$. Peaks at m/z 145 and 147 belong to the precursor, $C_6D_5COC\ell^+$. The acyl cation $C_6D_5CO^+$ at m/z 110 arises from ionization-dissociation of $C_6D_5COC\ell$. At low heat, the precursor has largely decomposed to form *o*-benzyne shown at m/z 80 (o-$C_6D_4^+$), carbon monoxide and hydrogen chloride; the latter two products have high ionization energies[91] [$IE(CO)=14.014\pm0.003$ eV and $IE(DC\ell)=12.744\pm0.009$ eV] that are beyond the range of the 118.2 nm laser. The small feature at m/z 52 corresponds to ionized diacetylene $(DC{\equiv}C{-}C{\equiv}CD)^+$. PIMS detection of acetylene is not possible with the 10.487 eV laser due to its high[92] ionization energy, $IE(HCCH)=11.4006\pm0.0006$ eV. The ion signal at m/z 52 suggests that a small amount of o-C_6D_4 has fragmented to form $DC{\equiv}C{-}C{\equiv}CD$ and $DC{\equiv}CD$. At medium heat more o-C_6D_4 decomposes, as demonstrated by the increased peak intensity of m/z 52 and decreased peak intensity of m/z 80. The PIMS spectra cannot distinguish the o-C_6D_4 species from its isomers (m-C_6D_4, p-C_6D_4, and $DCC{-}CD{=}CD{-}CCD$).

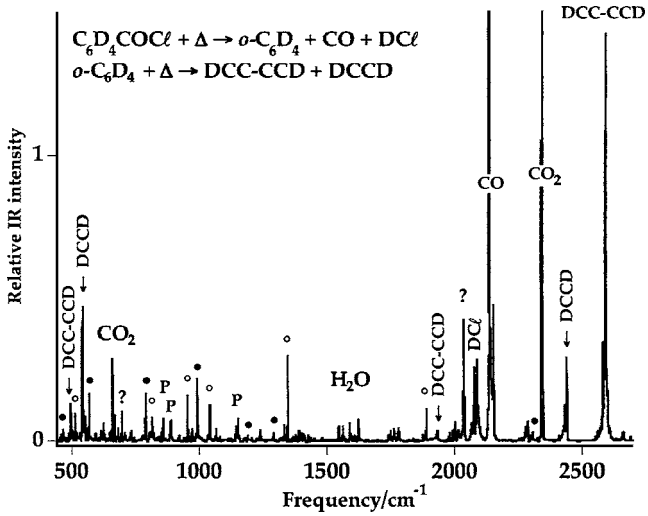

FIG. 2. Matrix-isolation IR spectrum from thermal decomposition of benzoyl-d_5 chloride at medium heat. The thermal decomposition products of benzoyl-d_5 chloride, *o*-benzyne, $DC\ell$, and CO, are observed. Also present in the spectrum are $DC{\equiv}C{-}C{\equiv}CD$ and $DC{\equiv}CD$, which are derived from o-C_6D_4 thermal fragmentation. A small amount of residual precursor is detected in the spectrum. Benzene-d_4 ($C_6H_2D_4$) which may arise from secondary reactions of *o*-benzyne-d_4 is also observed. The peak assignments (in cm^{-1}) follow. The unknown bands (indicated with ?) may result from impurities in the sample line or from the hot nozzle itself. o-C_6D_4 (●): 466, 569, 792, 993, 1191, 1292, 2307; $DC{\equiv}C{-}C{\equiv}CD$: 496, 1935, 2593; $DC{\equiv}CD$: 543, 2442; $C_6H_2D_4$ (○): 513, 816, 955, 1042, 1349, 1891; Unknown species (?): 699, 2037.

2. Matrix FTIR of $C_6D_5COC\ell$

Figure 2 is the IR absorption spectrum of the benzoyl chloride ($C_6D_5COC\ell$) pyrolysis products at medium heat (similar condition to the top trace of Fig. 1), which shows the generation[35] of o-C_6D_4 (marked by the bullets, •). Diacetylene and acetylene, which arise from further thermal cracking of o-C_6D_4, are prominent in the spectrum. There is still a small amount of the precursor remaining ($C_6D_5COC\ell$, marked by P), along with the benzene ($C_6D_4H_2$, marked by °) which may be produced from secondary reactions of o-C_6D_4. Signals from $DC\ell$ and CO (byproducts) are also detected as well as H_2O and CO_2 (from impurities).

3. Positive ion CIMS of benzoyl chloride pyrolysis

We have used a FA-SIFT device to study the reactions[45,46] of ions with *o*-benzyne. Figure 3 shows the reaction of H_3O^+ ions with the benzoyl chloride pyrolysis products at low and medium heat. The bottom trace is a reference spectrum resulting from reaction of mass-selected H_3O^+ and benzoyl chloride at room temperature; peaks at m/z 141, 143 are the protonated benzoyl chloride, $[C_6H_5COC\ell,H]^+$, at natural chlorine abundance. Fragmentation of these parent ions affords the acyl cation, $C_6H_5CO^+$ m/z 105 and $HC\ell$. At low heat, the major product is observed at m/z 77 ($C_6H_5^+$) which is derived from protonation

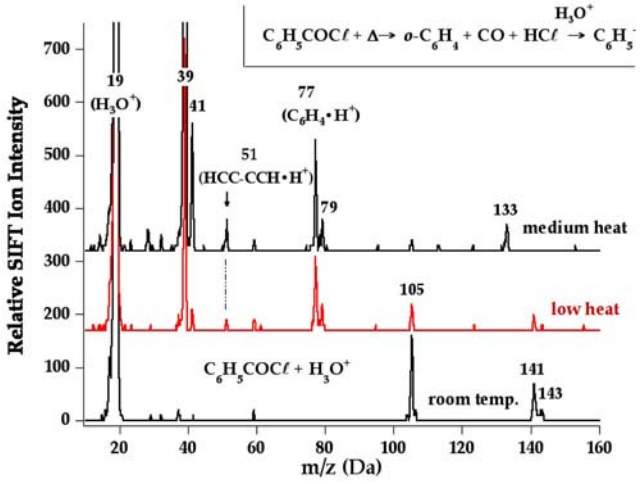

FIG. 3. SIFT mass spectrum for reaction of H_3O^+ with thermal decomposition products of benzoyl chloride at low and medium heat (top 2 traces). The signal at m/z 77 ($C_6H_5^+$) results from protonation of *o*-benzyne, $[o\text{-}C_6H_4,H^+]$. The peak at m/z 51 corresponds to protonated diacetylene $[HCCCCH,H^+]$. The bottom trace is a reference spectrum showing ions resulting from reaction of H_3O^+ and the precursor, benzoyl chloride. The peaks at m/z 39, 41, and 133 belong to K^+ and Cs^+, respectively, which come from the hot SiC nozzle itself.

of *o*-benzyne, $o\text{-}C_6H_4+H^+ \rightarrow [C_6H_4,H]^+$. A small amount of *o*-benzyne further fragments: $o\text{-}C_6H_4 \rightarrow HC{\equiv}CH$ and $HC{\equiv}C{-}C{\equiv}CH$. Acetylene (proton affinity[91] PA $=153.3$ kcal mol^{-1}) will not proton transfer with H_3O^+ but diacetylene[91] will ($PA=176.2$ kcal mol^{-1}) to produce the observed cation $[HC{\equiv}C{-}C{\equiv}CH,H^+]$ at m/z 51. At medium heat, the precursor benzoyl chloride is completely depleted, while protonated *o*-benzyne (m/z 77) and diacetylene (m/z 51) increase in intensity.

4. Negative ion CIMS of benzoyl chloride pyrolysis

Figure 4 displays the SIFT mass spectra for the reaction

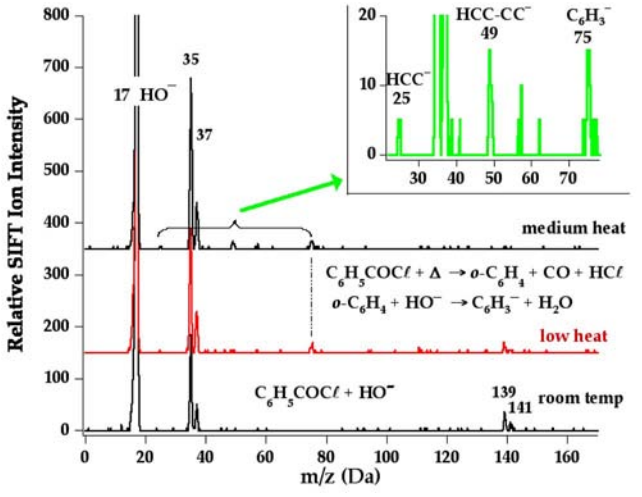

FIG. 4. SIFT mass spectrum for reaction of HO^- with thermal decomposition products of benzoyl chloride at low and medium heat (top 2 traces). The signal at m/z 75 ($C_6H_3^-$) results from deprotonation of *o*-benzyne. The peaks at m/z 49 and m/z 25 belong to the deprotonated diacetylene ($HCCCC^-$) and acetylene (HCC^-). The inset is an expanded view of the top trace from m/z 24 to 76. The bottom trace is a reference spectrum showing ions resulting from reaction of HO^- and the precursor, benzoyl chloride.

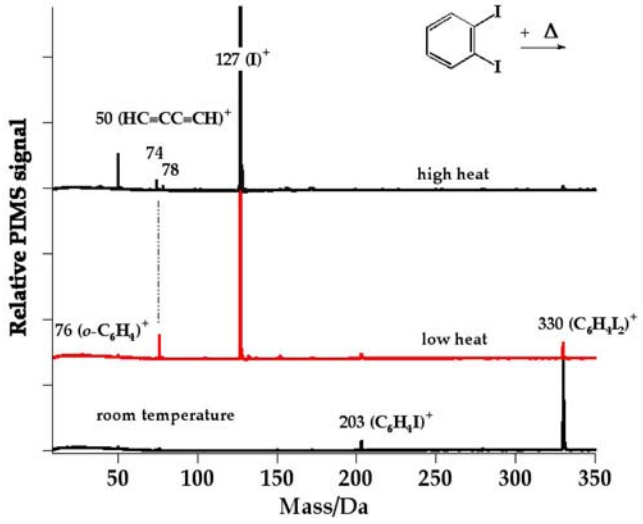

FIG. 5. TOF photoionization mass spectra from thermal decomposition of $C_6H_4I_2$. The reference spectrum with the nozzle unheated (room temperature) is also shown in the bottom trace. At room temperature, ions resulting from ionization of $C_6H_4I_2$ are detected: m/z 330 ($C_6H_4I_2^+$) and m/z 203 ($C_6H_4I^+$ from ionization-dissociation of $C_6H_4I_2$). At low heat, ions from thermal decomposition products are shown: *o*-benzyne at m/z 76 ($o\text{-}C_6H_4^+$) and iodine atom at m/z 127 (I^+). The signal at m/z 330 is attributed to residual precursor. At high heat, the peak at m/z 76 disappears while the peak at m/z 50 appears, which corresponds to ionized diacetylene $(HC{\equiv}C{-}C{\equiv}CH)^+$, indicating thermal cracking of *o*-benzyne. Small signals at m/z 74 and 78 most likely belong to $C_6H_2^+$ and $C_6H_6^+$ which may result from secondary reactions of $o\text{-}C_6H_4$.

of HO^- with benzoyl chloride pyrolysis products at low and medium heat. Hydroxide ion is very reactive since the gas-phase enthalpy of deprotonation[93,94] of water is $\Delta_{acid}H_{298}(HO{-}H)=390.20\pm0.07$ kcal mol^{-1}. The bottom trace is the reference spectrum resulting from reaction of mass-selected HO^- and the precursor, benzoyl chloride, at room temperature. Features at m/z 139, 141 are the deprotonated benzoyl chloride: $C_6H_5COC\ell+HO^- \rightarrow C_6H_4COC\ell^- +H_2O$. The large signal of $C\ell^-$ (m/z 35,37) results from a substitution reaction of benzoyl chloride with HO^-.

At low heat, the signal at m/z 75 ($C_6H_3^-$, 15 counts) is reproducibly observed, which is assigned to the deprotonated *o*-benzyne $[o\text{-}C_6H_3]^-$. At medium heat, benzoyl chloride is depleted, while deprotonated acetylene $HC{\equiv}C^-$ (m/z 25), diacetylene $HC{\equiv}C{-}C{\equiv}C^-$ (m/z 49), and *o*-benzyne $C_6H_3^-$ (m/z 75) are detected (see green inset). Both acetylene [gas-phase enthalpy of deprotonation[23] $\Delta_{acid}H_{298}(HCC{-}H)=378.3\pm0.1$ kcal mol^{-1}] and diacetylene[95] [$\Delta_{acid}H_{298}(HCCCC{-}H)=359\pm2$ kcal mol^{-1}] are thermal cracking products of $o\text{-}C_6H_4$.

5. TOF-PIMS of $o\text{-}C_6H_4I_2$

Figure 5 illustrates the TOF-PIMS spectrum of $o\text{-}C_6H_4I_2$ thermal decomposition. It demonstrates the production of $o\text{-}C_6H_4$, followed by cracking of $o\text{-}C_6H_4$ to form HCCH and HCC–CCH. The room temperature trace shows ions resulting from ionization of $o\text{-}C_6H_4I_2$; the peak at m/z 330 is $C_6H_4I_2^+$. The ion $C_6H_4I^+$ at m/z 203 arises from ionization-dissociation of $C_6H_4I_2$. At low heat, the precursor has largely decomposed to form *o*-benzyne shown at m/z 76 ($o\text{-}C_6H_4^+$) and iodine atom shown at m/z 127 (I^+). At high

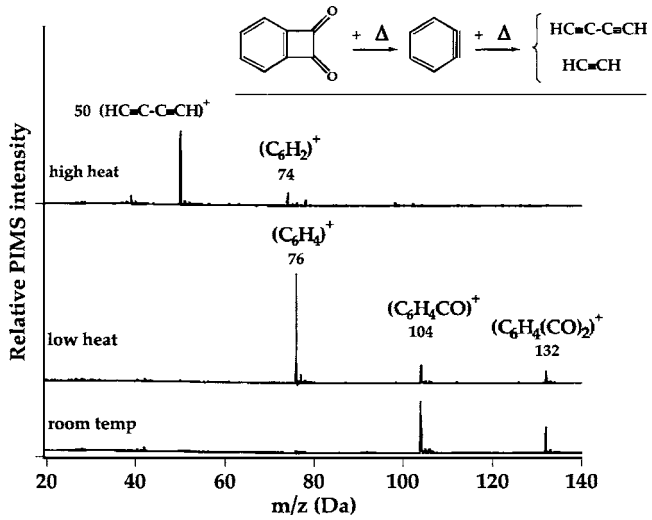

FIG. 6. TOF photoionization mass spectra from thermal decomposition of $C_6H_4(CO)_2$. The reference spectrum with the nozzle unheated (room temperature) is also shown in the bottom trace. At room temperature, ions resulting from ionization of $C_6H_4(CO)_2$ are detected: m/z 132 $[C_6H_4(CO)_2^+]$ and m/z 104 $[C_6H_4(CO)^+$ from ionization-dissociation of $C_6H_4(CO)_2]$. At low heat, thermal decomposition product *o*-benzyne shown at m/z 76 (o-$C_6H_4^+$) is observed. The signals at m/z 132 and 104 are attributed to residual precursor. At high heat, the peak at m/z 76 disappears while the peak at m/z 50 appears, which corresponds to ionized diacetylene $(HC{\equiv}C{-}C{\equiv}CH)^+$, indicating thermal cracking of *o*-benzyne. Two small signals at m/z 74 and 78 most likely belong to $C_6H_2^+$ and $C_6H_6^+$, which may result from secondary reaction of o-C_6H_4.

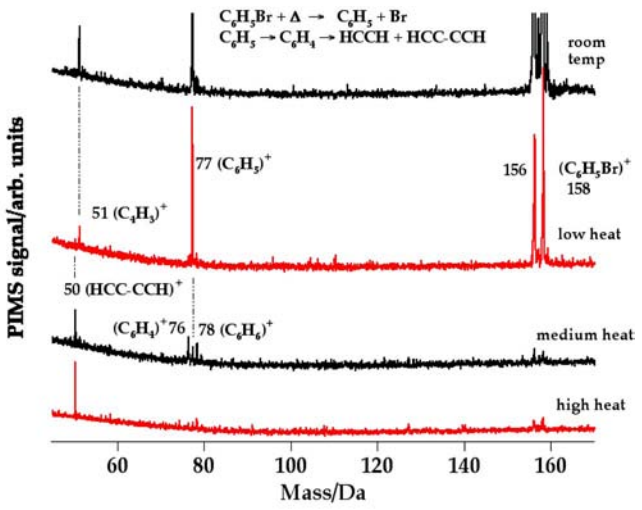

FIG. 7. TOF photoionization mass spectra from thermal decomposition of C_6H_5Br. The reference spectrum with the nozzle unheated (room temperature) is also shown in the top trace. At room temperature, ions resulting from ionization of C_6H_5Br are detected: m/z 156 and 158 ($C_6H_5Br^+$) as well as at m/z 77 and 51 ($C_6H_5^+$ and $C_4H_3^+$, respectively, from ionization-dissociation of C_6H_5Br). The intensities of the peaks at m/z 156 and 158 are about 20 times the intensities shown, and the peak height of m/z 77 is about twice as big as shown. At low heat, the thermal decomposition product, phenyl radical, is shown at m/z 77 ($C_6H_5^+$). The signals at m/z 156 and 158 are attributed to residual precursor. At medium heat, the peak at m/z 77 decreases while a new peak appears at m/z 50 corresponding to ionized diacetylene $(HC{\equiv}C{-}C{\equiv}CH)^+$, indicating thermal cracking of o-C_6H_4. *o*-Benzyne shown at m/z 76 can be generated by thermal dissociation of phenyl radical (C_6H_5). A small signal at 78 most likely belongs to $C_6H_6^+$ which may result from secondary reaction of C_6H_5. Both o-C_6H_4 and C_6H_6 may also be generated through disproportionation of C_6H_5. At high heat, the only peak remaining is m/z 50 $(HC{\equiv}C{-}C{\equiv}CH)^+$, indicating a complete thermal cracking of o-C_6H_4.

heat, o-C_6H_4 thermally decomposes to produce HCC–CCH and HCCH; the peak at m/z 50 corresponds to the diacetylene cation $(HC{\equiv}C{-}C{\equiv}CH)^+$.

6. TOF-PIMS of $C_6H_4(CO)_2$

Figure 6 displays the TOF-PIMS spectrum of the products of benzocyclobutene-1, 2-dione thermal decomposition. It demonstrates the clean production of o-C_6H_4, followed by fragmentation of o-C_6H_4 to form HCC–CCH and HCCH. At room temperature, two peaks appear: m/z 132 $C_6H_4(CO)_2^+$ belongs to the precursor and m/z 104 ($C_6H_4(CO)^+$) arises from ionization-dissociation of precursor $C_6H_4(CO)_2$. At low heat, the precursor has largely decomposed to form *o*-benzyne shown at m/z 76 (o-$C_6H_4^+$). At high heat, o-C_6H_4 is fragmented to form C_4H_2 and C_2H_2; the peak at m/z 50 corresponds to ionized diacetylene $(HC{\equiv}C{-}C{\equiv}CH)^+$.

7. TOF-PIMS of C_6H_5Br

Bromobenzene was used to generate the phenyl radical, which subsequently decomposes to *o*-benzyne. The o-C_6H_4 was observed to fragment further to acetylene and diacetylene.

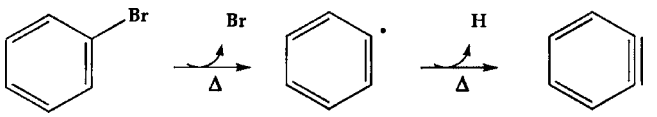

(12)

Figure 7 illustrates the TOF-PIMS spectrum of C_6H_5Br thermal decomposition. The room temperature spectrum at the top of Fig. 7 shows ions resulting from ionization of the precursor C_6H_5Br. The signals at m/z 156 and 158 belong to the precursor, $C_6H_5Br^+$. The features at m/z 77 ($C_6H_5^+$) and 51 ($C_4H_3^+$) arise from ionization-dissociation of C_6H_5Br. At low heat, the precursor has decomposed to form the phenyl radical shown at m/z 77 ($C_6H_5^+$) while bromine atom[96] has too high an ionization energy to be ionized by the 118.2 nm laser; $IE(\mathrm{Br}) = 11.813\,81 \pm 0.000\,06$ eV. Some of the precursor C_6H_5Br still remains as shown at m/z 156, 158, and 51. (It is likely that a small amount of signal at m/z 77 results from the precursor's ionization-dissociation.) At medium heat, the signal at m/z 77 ($C_6H_5^+$) decreases while new peaks at m/z 76 ($C_6H_4^+$) and 50 ($HCCCCH^+$) appear, indicating that phenyl radical further dissociates to form o-C_6H_4, which then fragments to HCC–CCH and HCCH. The bottom trace in Fig. 7 is at high heat and the only peak remaining is m/z 50 which corresponds to diacetylene ($HCC{-}CCH^+$). Matrix-isolation FTIR spectra of C_6H_5Br thermal decomposition were also collected and revealed signals from both HCCH and HCC–CCH, thus confirming the assignments for the TOF-PIMS experiment in Fig. 7. These IR spectra are not shown in this paper but are similar to Fig. 2.

B. Detection and thermal decomposition of 3,6-dimethyl-*o*-benzyne

1. PIMS of $2,5\text{-}(CH_3)_2C_6H_3COC\ell$

The mechanism for the fragmentation of *o*-benzyne to produce acetylene and diacetylene in Eq. (3) and Scheme I is an apparent retro-Diels-Alder reaction. These general reactions have been exhaustively studied.[97–100] It is believed that retro-Diels-Alder fragmentations are rapid, direct processes. This implies that the chemically activated *o*-benzyne fragments to acetylene and diacetylene without scrambling: $[o\text{-}C_6H_4]^* \rightarrow HC{\equiv}CH + HC{\equiv}C{-}C{\equiv}CH$.

In an attempt to test for a retro-Diels-Alder mechanism, we have examined the regiochemistry of the fragmentation of a substituted *o*-benzyne. We use 2,5-dimethylbenzoyl chloride $[2,5\text{-}(CH_3)_2C_6H_3COC\ell]$ as a precursor to generate 3,6-dimethyl-*o*-benzyne [Eq. (13)]. Scheme III indicates that this *o*-benzyne should fragment to form only acetylene ($HC{\equiv}CH$) and dimethyldiacetylene ($CH_3{-}C{\equiv}C{-}C{\equiv}C{-}CH_3$) [Eq. (14)].

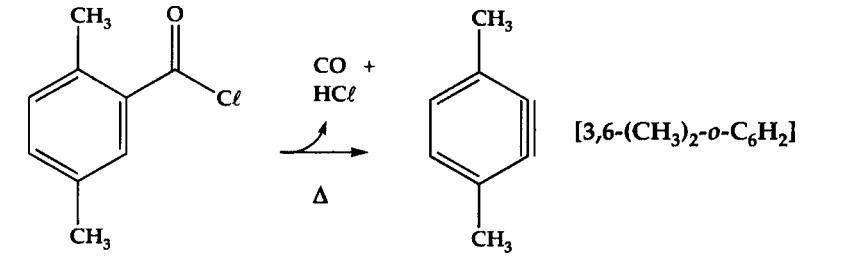

(13)

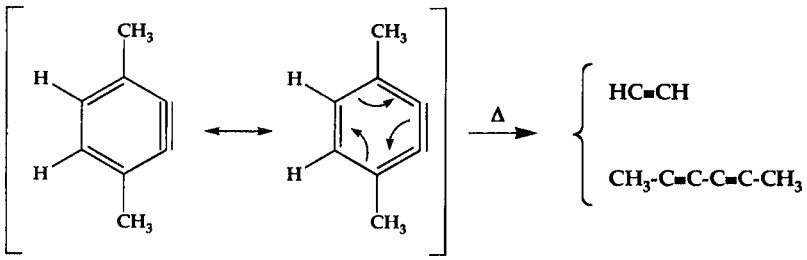

(14)

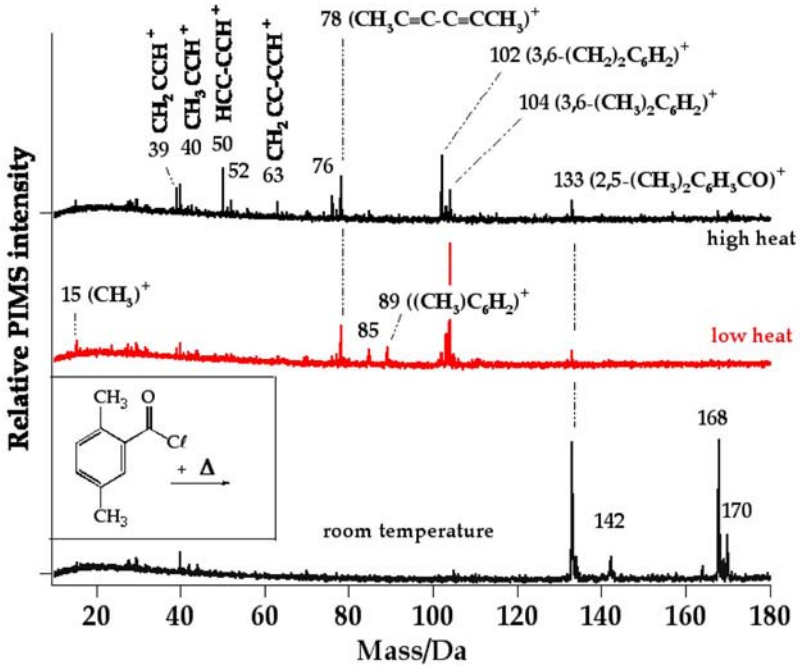

FIG. 8. TOF photoionization mass spectra from supersonic hyperthermal nozzle decomposition of $2,5\text{-}(CH_3)_2C_6H_3COC\ell$. The reference spectrum with the nozzle unheated (room temperature) is also shown in the bottom trace. At room temperature, ions resulting from ionization of $2,5\text{-}(CH_3)_2C_6H_3COC\ell$ are detected: m/z 168 and 170 $[2,5\text{-}(CH_3)_2C_6H_3COC\ell^+]$ as well as m/z 133 $[2,5\text{-}(CH_3)_2C_6H_3CO]^+$ from ionization-dissociation of $[2,5\text{-}(CH_3)_2C_6H_3COC\ell]$. At low heat thermal decomposition products are observed: m/z 104 $[3,6\text{-}(CH_3)_2\text{-}o\text{-}C_6H_2^+]$, m/z 78 $(CH_3C{\equiv}C{-}C{\equiv}CCH_3)^+$, m/z 15 (CH_3^+), m/z 89 $[6\text{-}(CH_3)\text{-}o\text{-}C_6H_2^+]$, m/z 103 $[3\text{-}(CH_2)\text{-}6\text{-}(CH_3)\text{-}o\text{-}C_6H_2^+]$. The small feature at m/z 85 is unknown. At high heat most of $3,6\text{-}(CH_3)_2\text{-}o\text{-}C_6H_2$ at m/z 104 further fragments to form $3,6\text{-}(CH_2)_2\text{-}o\text{-}C_6H_2$ shown at m/z 102, or acetylene and dimethyldiacetylene ($CH_3C{\equiv}C{-}C{\equiv}CCH_3$) at m/z 78 which can further dissociate to $CH_2{=}C{=}C{=}C{=}C{=}CH_2$ shown at m/z 76. The peaks at m/z 39, 40, and 63 correspond to $HCCCH_2$, methylacetylene, and $HCCCCCH_2$, respectively. The signals at m/z 50 and 52 correspond to diacetylene and H_2CCCCH_2.

Before discussing the experimental spectra, it is helpful to consider the implications from Scheme I which are sketched in Scheme III for the dimethylbenzynes.

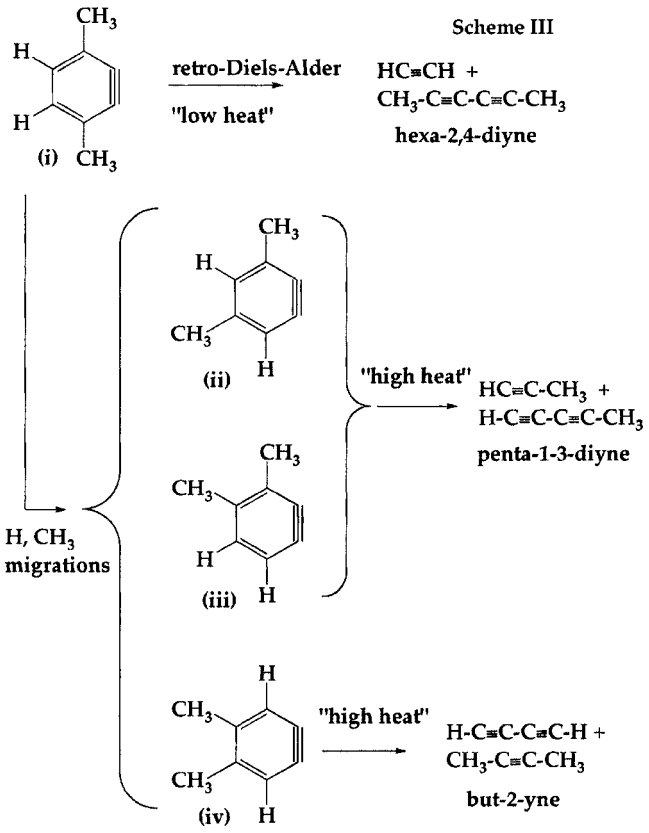

The nascent 3,6-$(CH_3)_2$-*o*-C_6H_2 (i, Scheme III) could directly fragment to $HCCH+CH_3CC-CCCH_3$. Alternatively 3,6-$(CH_3)_2$-*o*-C_6H_2 might rearrange to the less stable isomers, *m*-benzyne and *p*-benzyne, which cascade to a set of isomeric *o*-benzynes (ii, iii, and iv, Scheme III). Retro-Diels-Alder fragmentation of ii, iii, or iv would generate a different set of acetylene and diacetylene isomers.

Figure 8 plots the TOF-PIMS spectrum of 2,5-$(CH_3)_2C_6H_3COC\ell$ thermal decomposition products. It shows the production of 3,6-$(CH_3)_2$-*o*-C_6H_2, followed by its fragmentation to $CH_3C{\equiv}C-C{\equiv}CCH_3$ and $HC{\equiv}CH$. The bottom trace shows ions resulting from ionization of the precursor via a room temperature nozzle. Peaks at m/z 168 and 170 belong to the precursor $[2,5\text{-}(CH_3)_2C_6H_3COC\ell]^+$, while the ion $[2,5\text{-}(CH_3)_2C_6H_3CO]^+$ at m/z 133 arises from ionization-dissociation of the precursor. At low heat, the precursor has largely decomposed to form $[3,6\text{-}(CH_3)_2$-*o*-$C_6H_2]^+$ shown at m/z 104. Some cation further dissociates to form $(CH_3C{\equiv}C-C{\equiv}CCH_3)^+$ shown at m/z 78, and acetylene. A small amount of 3,6-$(CH_3)_2$-*o*-C_6H_2 also decomposes [see Eq. (15)] into $(CH_3)^+$ and (6-(CH_3)-*o*-$C_6H_2)^+$, which appear at m/z 15 and 89, respectively. The small peak at m/z 85 is unknown. The signal at m/z 103 results from the decomposition of 3,6-$(CH_3)_2$-*o*-C_6H_2 to H and 3-(CH_2)-6-(CH_3)-*o*-C_6H_2.

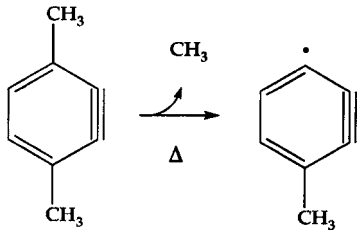

(15)

At high heat the cracking pattern of 3,6-$(CH_3)_2$-*o*-C_6H_2 becomes much more complex. The compound appears to fragment as shown in Eq. (16) to form the conjugated species 3,6-$(CH_2)_2$-*o*-C_6H_2.

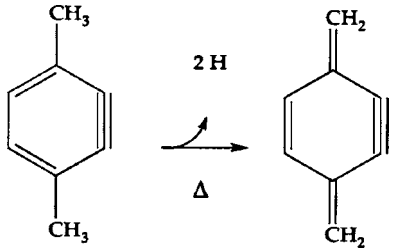

(16)

Retro-Diels-Alder fragmentation of the benzyne, 3,6-$(CH_3)_2$-*o*-C_6H_2, to acetylene and dimethyldiacetylene produces the $(CH_3-C{\equiv}C-C{\equiv}C-CH_3)^+$ ion at m/z 78. Dimethylacetylene can lose an additional pair of H atoms to generate the cumulated species, $CH_2{=}C{=}C{=}C{=}C{=}CH_2$. These mechanisms are consistent with the decreased peak intensity of m/z 104 $[3,6\text{-}(CH_3)_2$-*o*-$C_6H_2]^+$ and increased peak intensities of m/z 76 $(CH_2CCCCCH_2)^+$ and 102 $[3,6\text{-}(CH_2)_2$-*o*-$C_6H_2]^+$.

In addition to the retro-Diels-Alder cracking of the 3,6-$(CH_3)_2$-*o*-C_6H_2 benzyne, more complicated fragmentations are evident in the top trace of Fig. 8. As suggested in Scheme III, H and CH_3 migrations around the benzyne ring could form different benzyne isomers[5] which can further fragment to several products. The peaks at m/z 39, 40, and 63 belong to propargyl $(HCCCH_2)^+$, methylacetylene $(HC{\equiv}CCH_3)^+$, and $(HC{\equiv}C-C{\equiv}C-CH_2)^+$, respectively, which are fragmentation products of 3,4-dimethyl-*o*-benzyne and 3,5-dimethyl-*o*-benzyne. The signals at m/z 50 and 52 belong to $HC{\equiv}C-C{\equiv}CH$ and $CH_2{=}C{=}C{=}CH_2$ which are fragmentation products of 4,5-dimethyl-*o*-benzyne.

2. IR of 2,5-$(CH_3)_2C_6H_3COC\ell$

Figures 9(a) and 9(b) are the IR spectra of 2,5-dimethylbenzoyl chloride pyrolysis. Figure 9(a) shows the IR spectra in the low frequency fingerprint region. At room temperature, the signals belong to the precursor. At low heat, $HC{\equiv}CH$ and CH_3 are observed as well as 3,6-$(CH_3)_2$-*o*-C_6H_2. This demonstrates that the retro-Diels-Alder reaction of 3,6-dimethyl-*o*-benzyne occurs at relatively lower temperature. At medium heat, the acetylene peak increases while the methyl peak decreases and a feature which belongs to $CH_3C{\equiv}CH$ grows in. This is evidence for H or CH_3 migrations. At high heat the signals of CH_3, $HC{\equiv}CH$, and $CH_3C{\equiv}CH$ all disappear. However, a new peak which is assigned to $HC{\equiv}C-C{\equiv}CH$ appears; this is consistent with further H and CH_3 migrations.

Figure 9(b) displays the IR spectra in the high frequency C–H stretching region. At low heat, there are small signals that belong to HC≡CH and HC≡CCH$_3$. At medium heat, both the acetylene peak and the methylacetylene peak increase, and signals that belong to HC≡C–C≡CH and HCCCH$_2$ grow in. At high heat, both the acetylene peak and the methylacetylene peak decrease, while signals that belong to HC≡C–C≡CH and HCCCH$_2$ continue to increase. These results are in agreement with the findings obtained from the IR spectra in Fig. 9(a) and the PIMS spectrum in Fig. 8.

V. THEORETICAL ASSESSMENT OF BENZYNE FRAGMENTATION

We have used rigorous *ab initio* electronic structure computations to characterize the retro-Diels-Alder fragmentation of *o*-C$_6$H$_4$ to acetylene+diacetylene. Geometric structures fully optimized at our highest level of theory [explicit or composite CCSD(T)-AE/cc-pCVQZ] for *o*-benzyne, acetylene, diacetylene, and the retro-Diels-Alder transition state are shown in Figs. 10–12. A more extensive tabulation of r_e parameters for all these species at the RHF, MP2, CCSD, and CCSD(T) levels with the cc-pVDZ, cc-pVTZ, and cc-pCVQZ basis sets is provided as Supplementary Material.[101]

To complete the assessment of the thermochemistry of reaction (3), we require the heat of formation of diacetylene. A valence focal-point analysis of

$$2\mathrm{HCCH} \rightarrow \mathrm{HCC}\text{—}\mathrm{CCH} + \mathrm{H_2} \qquad (17)$$

was executed with cc-pV*X*Z basis sets and explicit electronic energies computed at the RHF (X=2–6), MP2 (X=2–6), CCSD (X=2–5), CCSD(T) (X=2–5), CCSDT (X=2), and CCSDT(Q) (X=2) levels of theory. Core correlation was accounted for with the CCSD(T)/cc-pCVTZ method; CCSD(T)/cc-pVTZ structures and harmonic vibrational frequencies were employed. The final result for the reaction enthalpy of Eq. (17) at 298 K is +0.6±0.3 kcal mol^{-1}. Adopting the experimental[102] $\Delta_f H_{298}$(HCCH) =54.4±0.2 kcal mol^{-1}, we thus obtain $\Delta_f H_{298}$(diacetylene) =109.4±0.3 kcal mol^{-1}. A full report and refinement of our analysis of the heat of formation of diacetylene will appear in a forthcoming paper.

The best computed [c~CCSD(T)-AE/cc-pCVQZ] equilibrium structure for *o*-C$_6$H$_4$ is displayed in Fig. 10. In *o*-benzyne the C≡C distance is shortened by 0.14 Å from the bond distance in benzene upon dehydrogenation. The precise equilibrium structure[103] for gas-phase C$_6$H$_6$ is: r_e(CC)=1.391±0.001 Å and r_e(CH)=1.080±0.002 Å. The other C–C distances in *o*-benzyne are within 0.014 Å of the benzene value. An r_e structure derived from microwave spectra of *o*-benzyne isotopologs has recently been reported,[29–31] and the experimental structural parameters are listed in the caption of Fig. 10. The agreement between c~CCSD(T)-AE/cc-pCVQZ theory and experiment is on the order of 0.001 Å for bond distances and 0.1° for bond angles. The lone outlier is θ_5, for which theory predicts an angle 0.7° less than the experimental value. The size of this disparity might suggest a reexamination of the microwave data for those isotopologs that fix the hydrogen closest to the strained triple bond. The electric dipole moment computed for *o*-benzyne with CCSD(T)/cc-pVTZ theory is μ_e(*o*-C$_6$H$_4$)=1.54 D.

The C–C≡C angle in *o*-benzyne is greater by almost 7° relative to benzene but is still more than 53° smaller than the idealized angle (180°) for *sp* hybridization. The resulting ring strain engenders diradical character in *o*-benzyne, amounting to about 10% of the ground-state singlet electronic wave function.[104] Nonetheless, this degree of multireference character can be readily described by single-reference coupled-cluster methods extended through connected triple excitations. This conclusion was confirmed by evaluation of a common T_1 coupled-cluster diagnostic[105] for *o*-benzyne, yielding 0.0130, comfortably below the recommended threshold of 0.020 for invoking multireference methods. The largest doubles (T_2) amplitude in the CCSD/cc-pVTZ wave function is 0.154, corresponding to the in-plane $\pi^2 \rightarrow \pi^{*2}$ excitation in the C≡C bond. No other T_2 amplitude exceeds 0.09.

For the acetylene+diacetylene fragmentation products (Fig. 12), the C≡C distances (1.204 and 1.209 Å) are now fully contracted to prototypical triple-bond lengths. The C–H distances in the products are about 0.02 Å shorter than in the *o*-benzyne reactant. Electron delocalization in diacetylene is evident in the unusually[106] short central C–C bond length of 1.374 Å as well as a surprisingly strong C–C bond energy. With our best computed $\Delta_f H_{298}$(HCC–CCH) of 109.4±0.3 kcal mol^{-1}, one finds DH_{298}(HCC–CCH) =161.9±0.6 kcal mol^{-1}. Recall[14] that a typical "sp^3 C–C bond strength" is DH_{298}(CH_3CH_2–CH_2CH_3) =88.0±0.6 kcal mol^{-1} while a common "sp^2 C–C bond strength" is DH_{298}(CH_2CH–$CHCH_2$)=116±1 kcal mol^{-1}. The normal >C═C< bond energy is 174 kcal mol^{-1} (from ethylene)[14] and a typical –C≡C– bond energy is 230 kcal mol^{-1} (from acetylene).[14] However, the DH_{298}(HCCCC–H) has been measured[95] to be identical to that of DH_{298}(HCC–H).

A comparison of the explicit CCSD(T)-AE/cc-pCVQZ bond distances for acetylene with r_e parameters derived from high-resolution IR spectroscopy [r_e(C≡C) =1.202 92±0.000 13 Å, r_e(C–H)=1.061 38±0.000 35 Å][107] shows remarkable accord, with disparities of only +0.0008 and +0.0007 Å, respectively. This impressive performance of the CCSD(T)-AE/cc-pCVQZ method is a general occurrence.[108] As documented in the Supplementary Material,[101] the composite c~CCSD(T)-AE/cc-pCVQZ approach is able to reproduce the explicit CCSD(T)-AE/cc-pCVQZ results for all bond distances in acetylene and diacetylene to 0.0002 Å or better. This comparison places a high degree of confidence in the c~CCSD(T)-AE/cc-pCVQZ structures of *o*-benzyne and the retro-Diels-Alder transition state. The (CCSD/cc-pVTZ) T_1 diagnostics for acetylene and diacetylene are 0.0132 and 0.0139, respectively. By this measure, the overall multireference character in the *o*-benzyne reactant is very nearly the same (actually slightly smaller) as in the fragmentation products.

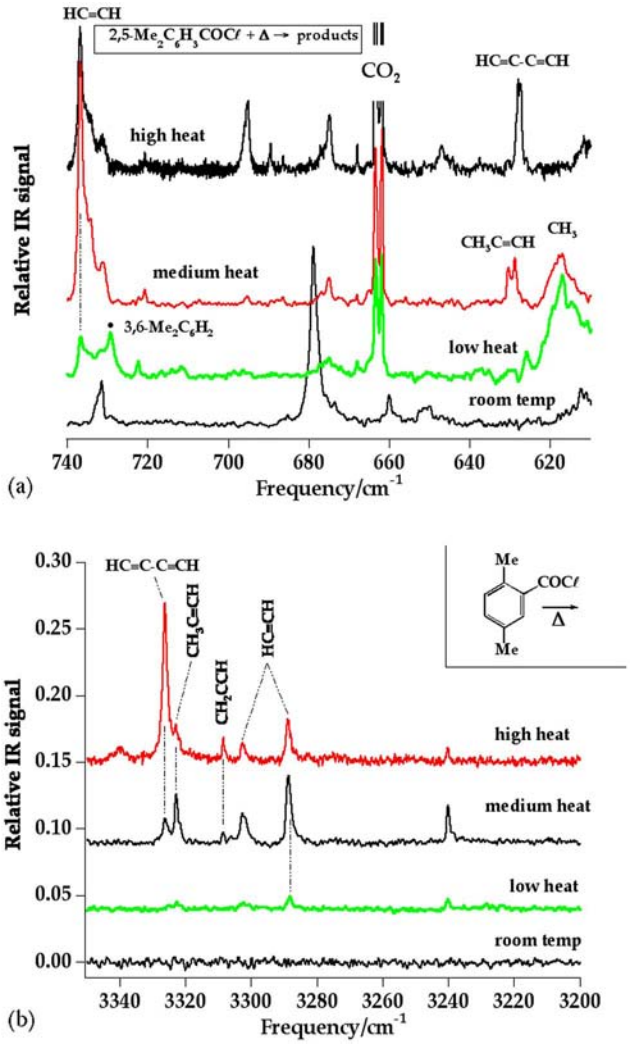

FIG. 9. (a) IR spectra of 2,5-$(CH_3)_2C_6H_3COC\ell$ pyrolysis in the low frequency fingerprint region. At room temperature, the signals correspond to the precursor. At low heat HCCH and CH_3 are observed as well as 3,6-$(CH_3)_2$-*o*-C_6H_2. At medium heat, the HCCH peak increases while CH_3 decreases and a new peak (CH_3CCH) appears. At high heat signals of methyl radical and methylacetylene disappear, the acetylene peak decreases, and a new peak corresponding in HCC–CCH appears. (b) IR spectra of 2,5-$(CH_3)_2C_6H_3COC\ell$ pyrolysis at relatively high frequency C–H stretching region. At low heat, there are small signals that correspond to acetylene and methylacetylene. At medium heat, both of these peaks increase, and signals that correspond to diacetylene and propargyl radical ($HCCCH_2$) appear. At high heat, both the acetylene peak and the methylacetylene peak decrease, while signals that correspond to diacetylene and propargyl radical increase.

The retro-Diels-Alder fragmentation of *o*-benzyne is formally allowed by conservation of orbital symmetry,[109] as the number of (a_1,a_2,b_1,b_2) doubly occupied valence orbitals is (7, 1, 2, 4) in both the reactant and products for the C_{2v} path A. The principal orbital transformation is σ(C–C) (a_1,b_2) *o*-benzyne $\rightarrow \pi(a_1)$ acetylene $+\pi(b_2)$ diacetylene. From a frontier orbital perspective, the reverse reaction is driven by the interaction of $[\pi(a_1)\ C_2H_2,\ \pi^*(a_1)\ C_4H_2]$ and $[\pi^*(b_2)\ C_2H_2,\ \pi(b_2)\ C_4H_2]$ occupied/virtual orbital pairs.

In the C_{2v} transition state for concerted *o*-benzyne decomposition (Fig. 11), the C–C bond being broken has a distance of 2.198 Å at the c~CCSD(T)-AE/cc-pCVQZ level. As shown below, the transition state and products lie

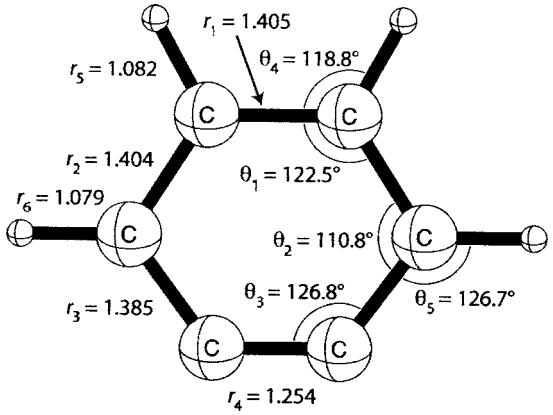

FIG. 10. c~CCSD(T)-AE/cc-pCVQZ optimum geometry (Å or deg) of *o*-benzyne. Experimental microwave values (Refs. 30 and 31) are $r_1=1.405\pm0.003$ Å, $r_2=1.403\pm0.002$ Å, $r_3=1.383\pm0.002$ Å, $r_4=1.255\pm0.003$ Å, $r_5=1.082\pm0.001$ Å, $r_6=1.080\pm0.001$ Å; $\theta_1=122.36°\pm0.08°$, $\theta_2=111.0°\pm0.1°$, $\theta_3=126.66°\pm0.09°$, $\theta_4=118.73°\pm0.08°$, and $\theta_5=127.40°\pm0.11°$.

94.5 and 59.8 kcal mol^{-1}, respectively, above *o*-benzyne, without inclusion of ZPVE. Our best computations place the transition state farther out in the product channel than in previous theoretical work: HF/6-31G(*d*), r(C···C) =2.148 Å; CASSCF(12,12)/6-31G(*d*,*p*), r(C···C) =2.147 Å;[5] and MP2/6-31G(*d*), r(C···C)=2.195 Å.[5] From the tabulations in Supplementary Material,[101] the [RHF, MP2, CCSD, CCSD(T)] series of r(C···C) distances (in Å) is (2.149, 2.221, 2.197, 2.233) and (2.132, 2.205, 2.171, 2.207) with the cc-pVDZ and cc-pVTZ basis sets, respectively. Thus, the transition state migrates outward in an oscillatory fashion with improvements in the electron correlation treatment but moves inward as the basis set is enlarged.

As expected for an endoergic reaction, the concerted retro-Diels-Alder reaction has a rather late transition state. As quantified by the (monotonic) progression of the C–C and C–H bond distances, the transition state occurs when the reaction is (75±7)% complete. However, the geometric relaxation necessary to yield the products is still substantial; for example, the C−C≡C angle must increase by 38.2° to reach linear diacetylene. If free acetylene and diacetylene are

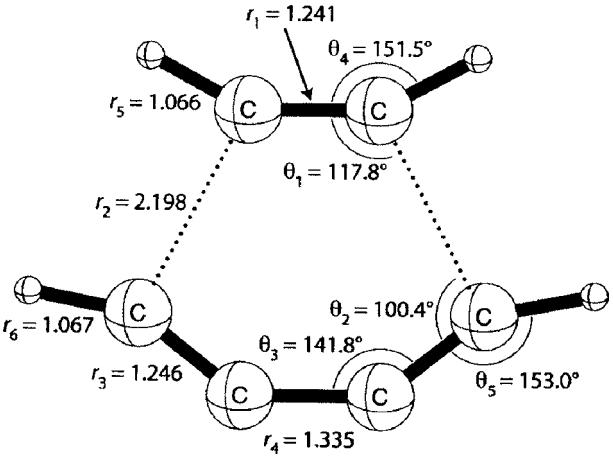

FIG. 11. c~CCSD(T)-AE/cc-pCVQZ optimum geometry (Å or deg) of C_{2v}-symmetric, retro-Diels-Alder transition state for concerted fragmentation of *o*-benzyne to acetylene+diacetylene.

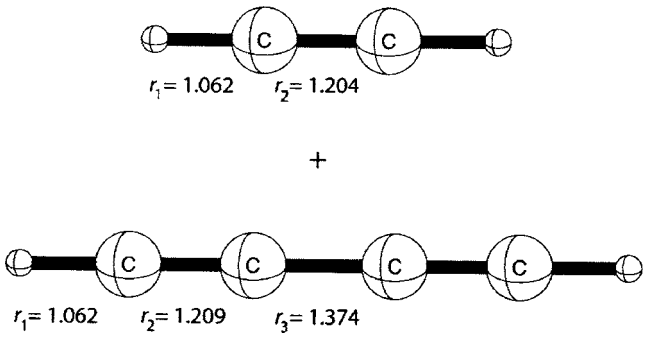

FIG. 12. CCSD(T)-AE/cc-pCVQZ optimum geometries (Å) of acetylene and diacetylene. From an analysis of high-resolution infrared absorption spectra (Ref. 107), the structure of acetylene is known to be r_e(C−H) = 1.061 38 ± 0.000 35 Å and r_e(C≡C) = 1.202 92 ± 0.000 13 Å. Alternative (Ref. 108) empirical r_e parameters are r_e(C≡C) = 1.2026 Å, r_e(C−H) = 1.0622 Å.

distorted to the conformations taken by the corresponding fragments in the transition state, then the monomer energies are raised by 12.7 and 25.8 kcal mol^{-1}, respectively, giving a total deformation energy of 38.5 kcal mol^{-1}, all at the CCSD(T)/cc-pVTZ level. In the process, the highest occupied molecular orbital (HOMO)/lowest unoccupied molecular orbital (LUMO) gaps of HCCH and HCC–CCH are reduced by 34.9 and 34.7 kcal mol^{-1}, respectively, preparing the frontier orbitals for bonding vis-à-vis the reverse reaction. The total deformation energy of the acetylene and diacetylene fragments is remarkably close to the corresponding CCSD(T)/cc-pVTZ barrier height (35.3 kcal mol^{-1}) for the reverse reaction, revealing that only 3.3 kcal mol^{-1} of electronic stabilization is gained in the transition state by interfragment orbital interactions.

The concerted (C_{2v}) retro-Diels-Alder transition state exhibits little multireference character, a conclusion critical for establishing the reliability of our computations. The [CCSD(T)/cc-pVTZ] T_1 diagnostic is 0.0148, only 6% larger than the value for diacetylene. The largest doubles (T_2) amplitude is only 0.089, comparable to those in acetylene and diacetylene and substantially smaller than that in *o*-benzyne. In our CASSCF(12,12)/cc-pVDZ computations at the CCSD(T)/cc-pVTZ geometry, the four largest configuration interaction (CI) coefficients ranged from 0.102 to 0.131, and the natural orbital occupation numbers in the Hartree-Fock virtual space never exceeded 0.112. Such CI coefficients are typical of CASSCF computations on single-reference systems. In brief, a number of measures show that there are no secondary reference configurations of importance for the transition state, and the CCSD(T) method should provide a highly accurate description in this region of the potential energy surface.

To obtain final energetics for the retro-Diels-Alder decomposition of *o*-benzyne, focal-point analyses were executed for the reaction energy and the fragmentation barrier. The layout of the dual approach to the one- and *N*-particle limits is provided in Table I. There is very little uncertainty in achieving the CBS limit of each electronic structure method, as the extrapolated increments are all within 0.25 kcal mol^{-1} of the largest explicitly computed values. On the other hand, the approach to the full configuration interaction (FCI) limits is oscillatory and more demanding to converge. With the cc-pVDZ basis set, the [MP2, CCSD, CCSD(T), CCSDT(Q)] correlation increments for the reaction energy are (+23.00, −7.98, +4.41, −0.17) kcal mol^{-1}, and those for the barrier height are (−13.26, +5.39, −2.49, −0.28) kcal mol^{-1}. Based on these trends, we conservatively ascribe uncertainties of ±0.5 kcal mol^{-1} to the CCSDT(Q) values for the reaction energy and barrier height as estimates of the FCI limit. The valence focal-point analyses yield final results of (59.9, 94.2) kcal mol^{-1} for ($\Delta E_{\rm rxn}, \Delta E_b$), whereas all-electron computations at the CCSD(T)/cc-pCVTZ level give core-correlation shifts of (−0.08, +0.26) kcal mol^{-1}. With addition of the large effect of zero-point vibrations [evaluated from unscaled CCSD(T)/cc-pVTZ harmonic vibrational frequencies], our final predictions from Table I of the *ab initio* limits are $\Delta E_{\rm rxn,0}$ = 52.4 ± 0.5 kcal mol^{-1} and $\Delta E_{b,0}$ = 88.0 ± 0.5 kcal mol^{-1}, both quantities corresponding to 0 K. With CCSD(T)/cc-pVTZ thermal corrections, the reaction energy at 298 K becomes 55.2 ± 0.5 kcal mol^{-1}. Using our computed $\Delta_f H_{298}$(diacetylene) from above and experimental values for *o*-C_6H_4 and HCCH, the "experimental" $\Delta_{\rm rxn} H_{298}$(*o*-$C_6H_4 \rightarrow$ HC≡CH + HC≡C−C≡CH) becomes 57 ± 3 kcal mol^{-1}. The purely *ab initio* and experimental reaction energies for *o*-benzyne decomposition are in satisfactory accord.

In 1999, Moskaleva *et al.*[5] studied the decomposition and isomerization of *o*-benzyne with the composite G2M(rcc, MP2) method.[110] The highest-level single-point energies in this scheme are determined from RCCSD(T)/6-311G(*d*,*p*) and MP2/6-311+G(3*df*,2*p*) computations. In the standard G2M(rcc, MP2) approach, the geometries and vibrational frequencies are determined from B3LYP/6-311G(*d*,*p*) density functional theory; however, there is no C_{2v}-symmetric retro-Diels-Alder transition state for this method, and thus MP2/6-31G(*d*) was substituted for the geometry optimizations. With inclusion of ZPVE, the G2M(rcc, MP2) results for the 0 K retro-Diels-Alder (fragmentation energy, barrier height) were (50.2, 87.4) kcal mol^{-1}. An earlier 1998 study[4] at the less reliable B3LYP/6-31G*//HF/6-31G* level placed the barrier height at 88.6 kcal mol^{-1}. The previous theoretical data of Refs. 4 and 5 agree with our new results within 2.5 kcal mol^{-1}. In contrast, the barrier height reported in 2000 by Wang *et al.*[6] is 4–5 kcal mol^{-1} smaller than our final value.[111]

Vibrational frequencies at the CCSD(T)/cc-pVTZ level for *o*-benzyne, acetylene, diacetylene, and the concerted (C_{2v}) retro-Diels-Alder transition state are compiled in Table II. Corresponding CCSD(T)/cc-pVDZ frequencies are given in Supplementary Material.[101] The frequencies of 20 of the 24 internal vibrations transform monotonically along the path, including the modes correlating to C≡C stretches in acetylene and diacetylene, i.e., [$\omega_9(a_1)$: 1904 → 2015 → 2233 cm^{-1}]; [$\omega_4(a_1)$: 1477 → 1750 → 2201 cm^{-1}]; and [$\omega_{19}(b_2)$: 1488 → 1854 → 2051 cm^{-1}]. The most salient frequencies in Table II are $\omega_9(a_1) = 621i$ cm^{-1} and $\omega_{24}(b_2)$ = 40 cm^{-1} in the transition state, the associated normal modes being depicted in Fig. 13. The $\omega_9(a_1)$ eigenvector gives positive identification of the retro-Diels-Alder transi-

TABLE I. Valence focal-point analysis of the reaction energy and concerted retro-Diels-Alder barrier for the fragmentation of *o*-benzyne to acetylene and diacetylene. The symbol δ denotes the *increment* in the energy difference (ΔE) with respect to the previous level of theory. Bracketed numbers are the result of basis set extrapolations or additivity assumptions (as specified at the bottom of the table), while unbracketed numbers were explicitly computed. The reference structures were the CCSD(T)-AE/cc-pCVQZ optimized geometries depicted in Figs. 10–12. The use of CCSD(T)/cc-pVTZ structures changes the final energetics by no more than 0.1 kcal mol^{-1}.

Basis set	ΔE_e[RHF]	$+\delta$[MP2]	$+\delta$[CCSD]	$+\delta$[CCSD(T)]	$+\delta$[CCSDT(Q)]	ΔE_e[CCSDT(Q)]
			Fragmentation energy (ΔE_{rxn}, kcal mol^{-1})			
cc-pVDZ	44.27	+23.00	−7.98	+4.41	−0.17	63.52
cc-pVTZ	38.45	+24.80	−9.11	+4.66	[−0.17]	[58.63]
cc-pVQZ	38.47	+25.34	−9.13	+4.78	[−0.17]	[59.28]
cc-pV5Z	38.59	+25.55	[−9.16]	[+4.82]	[−0.17]	[59.63]
cc-pV6Z	38.62	+25.59	[−9.12]	[+4.84]	[−0.17]	[59.76]
CBS limit	[38.63]	[+25.71]	[−9.13]	[+4.87]	[−0.17]	**[59.91]**

$\Delta E_{rxn,0}$(final) = ΔE_e[CBS CCSDT(Q)] + ΔZPVE[CCSD(T)/cc-pVTZ] + Δcore[CCSD(T)/cc-pCVTZ]
= 59.91 − 7.46 − 0.08 = **52.4 ± 0.5 kcal mol^{-1}**

			Barrier (ΔE_b, kcal mol^{-1})			
cc-pVDZ	108.43	−13.26	+5.39	−2.40	−0.28	97.88
cc-pVTZ	104.83	−14.28	+6.41	−2.89	[−0.28]	[93.79]
cc-pVQZ	104.87	−14.40	+6.86	−3.05	[−0.28]	[94.01]
cc-pV5Z	104.98	−14.42	[+6.99]	[−3.10]	[−0.28]	[94.17]
cc-pV6Z	104.99	−14.42	[+7.04]	[−3.13]	[−0.28]	[94.21]
CBS limit	[104.99]	[−14.43]	[+7.11]	[−3.16]	[−0.28]	**[94.24]**

$\Delta E_{b,0}$(final) = ΔE_e[CBS CCSDT(Q)] + ΔZPVE[CCSD(T)/cc-pVTZ] + Δcore[CCSD(T)/cc-pCVTZ]
= 94.24 − 6.52 + 0.26 = **88.0 ± 0.5 kcal mol^{-1}**

Fit	$a+bc^{-cX}$	$a+bX^{-3}$	$a+bX^{-3}$	$a+bX^{-3}$	additive
Points (X)	4,5,6	4,5,6	3,4	3,4	

tion state, whereas the $\omega_{24}(b_2)$ eigenvector is a distortion toward a stepwise carbon-carbon bond fragmentation path.

The potential energy curve along the $\omega_{24}(b_2)$ normal mode is extremely flat. Indeed, some lower levels of theory give imaginary values of $\omega_{24}(b_2)$, a fact observed for B3LYP/6-311G(d,p) theory by Moskaleva *et al.*[5] but whose significance was not pursued. With the cc-pVDZ basis set, we find $\omega_{24}(b_2)=(177,178,39,93i)$ cm^{-1} at the [RHF, MP2, CCSD, CCSD(T)] levels. To gain more confidence that the concerted, retro-Diels-Alder process (path A) has a true transition state in C_{2v} symmetry with a single imaginary frequency corresponding to $\omega_9(a_1)$, we recomputed the b_2 vibrational frequencies of the critical structure at the c∼CCSD(T)-AE//cc-pCVQZ level. As a test of our procedure, we obtained the following frequencies (in cm^{-1}) for acetylene: $[\omega_1(\sigma_g),\omega_3(\sigma_u),\omega_2(\sigma_g),\omega_5(\pi_u),\omega_4(\pi_g)]$ = (3508, 3416, 2013, 748, 606) from explicit CCSD(T)-AE//cc-pCVQZ, and (3508, 3415, 2012, 746, 600) from c∼CCSD(T)-AE//cc-pCVQZ, as compared to (3501.5, 3417.6, 2013.3, 746.8, 621.5) from experiment.[112] The *o*-benzyne transition state frequencies given in parentheses in Table II show no asymmetric b_2 normal modes of negative curvature at the c∼CCSD(T)-AE//cc-pCVQZ level, and $\omega_{24}(b_2)$ has increased slightly to 42 cm^{-1}. In conclusion, we believe that the C_{2v} structure of Fig. 11 is stable with respect to all asymmetric distortions of the nuclear framework and is a genuine transition state for the C_{2v}-symmetric, concerted retro-Diels-Alder decomposition of *o*-benzyne (path A).

Notwithstanding the existence of path A, the remarkably flat $\omega_{24}(b_2)$ potential energy profile in the C_{2v} transition state raises the specter of more convoluted routes and complex dynamics for *o*-benzyne fragmentation. The qualitative energy contour sketches of Figs. 14 and 15 illustrate the most viable possibilities. Hypothetical path B is an asymmetric, but concerted, retro-Diels-Alder route having degenerate planar transition states of C_s symmetry. Path B might exist regardless of whether path A exhibits a true transition state. However, the scenario shown in Fig. 14 is more likely, whereby path A directly bifurcates into a degenerate path B pair when a mound (shown with a dashed contour) on the potential energy surface obstructs the C_{2v} route. We examined the possibility of path B by following the $\omega_{24}(b_2)$ normal mode with CCSD/cc-pVDZ theory. What we found was not a path B transition state, but one leading from *o*-benzyne to an open-chain, open-shell singlet intermediate HC$\overset{\cdot\cdot}{=}$C$\overset{\cdot\cdot\cdot}{-}$C=CH−CH=CH$\cdot$ which could subsequently undergo C–C bond scission to yield acetylene and diacetylene. Therefore, our computations do not support the existence of path B, but rather the nonconcerted path C depicted in Fig. 15, which might be a legitimate alternative for producing acetylene+diacetylene from *o*-benzyne.

The possible competition between paths A and C cannot be probed by any of the experiments reported in this paper. Furthermore the accurate theoretical characterization of path C is a formidable task that will require much additional computational effort. The severe multireference electronic char-

acter encountered along path C is an acute problem. Not only is the open-chain intermediate a large singlet diradical, but it is connected smoothly to closed-shell reactants and products via homolytic bond fission processes. We confirmed the difficulty of applying single-reference electron correlation methods to path C in locating the CCSD/cc-pVDZ transition state connecting *o*-benzyne to HC$\overset{\cdot\cdot}{=}$C$\overset{\cdot\cdot\cdot}{-}$C=CH−CH=CH·. The T_1 diagnostic (0.0585) for this transition state is enormous. The corresponding barrier for the first step of path C was almost 10 kcal mol^{-1} lower than the barrier for path A, but this prediction is likely dubious. Even if the first step of path C has a lower barrier than path A, the second step leading from the intermediate to acetylene+diacetylene fragments might be energetically prohibitive. Careful work with multireference and perhaps spin-flip coupled-cluster methods will be required to reliably investigate the possibility of a competitive, stepwise fragmentation path to acetylene and diacetylene.

Constructing multiconfigurational reference wave functions for characterization of paths A and C is also problematic. The σ(C−C) bonds in *o*-benzyne that are broken in the retro-Diels-Alder fragmentation have molecular orbitals buried below a σ(C−H) orbital. The correlating σ^*(C−C) virtual orbitals in *o*-benzyne have eight other virtual orbitals lower in energy, and, in particular, there are four σ^*(C−H) orbitals underneath. Accordingly, there are numerous avoided crossings in the orbital stacking as one proceeds from *o*-benzyne to the products via path A or C. Because of the cascading effect in the orbital transformations, there is no clear choice of a CASSCF scheme to describe the fragmentation process uniformly from reactant to products.

We have considered whether triplet electronic states might play a role in *o*-benzyne pyrolysis. The measured[34] singlet-triplet splitting in *o*-benzyne is 37.8±0.6 kcal mol^{-1}, whereas the lowest triplet electronic states in acetylene[113] and diacetylene[114,115] have adiabatic excitation energies of 88 and 62 kcal mol^{-1}, respectively. At the retro-Diels-Alder transition state, UMP2/cc-pVTZ theory places the lowest triplet state 134 kcal mol^{-1} above the ground-state singlet. Therefore, as long as the reaction dynamics proceed along the C_{2v} concerted path, rather than through open-chain intermediates, intersystem crossing to triplet surfaces is not a concern. However, the intermediate region of path C is certainly complicated by an intermingling of close-lying singlet and triplet states.

A pathway competitive to the decomposition of *o*-benzyne to acetylene and diacetylene is successive isomerization to *m*- and *p*-benzyne followed by a retro-Bergman[7,8] ring opening to hex-3-ene-1,5-diyne (HCC−CH=CH−CCH); see Scheme I. With G2M(rcc, MP2) theory[5] the transition states for *o*-benzyne → *m*-benzyne, *m*-benzyne → *p*-benzyne, and *p*-benzyne → hex-3-ene-1,5-diyne were computed to lie 71, 75, and 43 kcal mol^{-1}, respectively, above *o*-benzyne. While these energetics should be confirmed with higher levels of theory, it appears that the stepwise *o*-benzyne isomerization route has an overall barrier at least 10 kcal mol^{-1} below that for decomposition to acetylene+diacetylene via path A. Multichannel Rice-Ramsperger-Kassel-Marcus (RRKM)calculations[5] using G2M(rcc, MP2) potential energy surface data predict that the isomerization process accounts for as much as 99% of *o*-benzyne depletion at 1000 K. However, at temperatures above 2000 K concerted decomposition to acetylene and diacetylene dominates. Because our experiments are performed at temperatures between these two extremes, the isomerization and decomposition routes should be in strong competition. The crux is that the observed acety-

TABLE II. CCSD(T)/cc-pVTZ vibrational frequencies (in cm^{-1}) along the retro-Diels-Alder fragmentation path of *o*-benzyne. For the b_2 normal modes, c ~ CCSD(T)-AE/cc-pCVQZ frequencies are given in parentheses.

Mode	*o*-benzyne	Transition state	Products
$\omega_1(a_1)$	3220	3418	3511 (σ_g C_2H_2)
$\omega_2(a_1)$	3191	3380	3458 (σ_g C_4H_2)
$\omega_3(a_1)$	1904	2015	2233 (σ_g C_4H_2)
$\omega_4(a_1)$	1477	1750	2001 (σ_g C_2H_2)
$\omega_5(a_1)$	1318	1113	887 (σ_g C_4H_2)
$\omega_6(a_1)$	1154	850	746 (π_u C_2H_2)
$\omega_7(a_1)$	1055	699	633 (π_u C_4H_2)
$\omega_8(a_1)$	996	404	227 (π_u C_4H_2)
$\omega_9(a_1)$	606	621*i*	0
$\omega_{10}(a_2)$	949	624	623 (π_g C_4H_2)
$\omega_{11}(a_2)$	862	597	578 (π_g C_2H_2)
$\omega_{12}(a_2)$	592	487	474 (π_g C_4H_2)
$\omega_{13}(a_2)$	440	254	0
$\omega_{14}(b_1)$	914	658	746 (π_u C_2H_2)
$\omega_{15}(b_1)$	746	622	633 (π_u C_4H_2)
$\omega_{16}(b_1)$	387	228	227 (π_u C_4H_2)
$\omega_{17}(b_2)$	3216	3380 (3385)	3454 (σ_u C_4H_2)
$\omega_{18}(b_2)$	3174	3355 (3357)	3410 (σ_u C_2H_2)
$\omega_{19}(b_2)$	1488	1854 (1866)	2051 (σ_u C_4H_2)
$\omega_{20}(b_2)$	1418	838 (838)	623 (π_g C_4H_2)
$\omega_{21}(b_2)$	1261	746 (757)	578 (π_g C_2H_2)
$\omega_{22}(b_2)$	1107	483 (489)	0
$\omega_{23}(b_2)$	849	435 (442)	474 (π_g C_4H_2)
$\omega_{24}(b_2)$	462	40 (42)	0

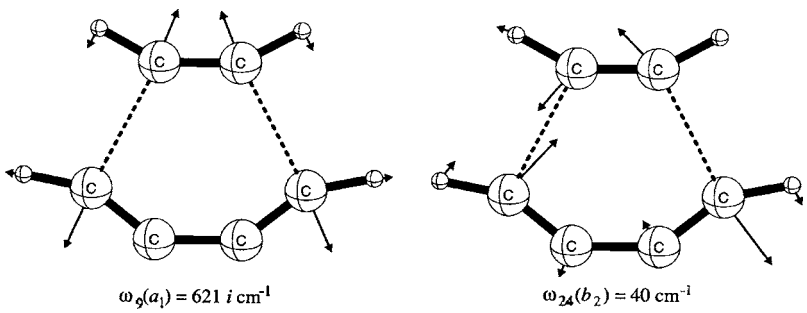

FIG. 13. Normal-mode eigenvectors [$Q_9(a_1)$ and $Q_{24}(b_2)$] for the retro-Diels-Alder transition state for *o*-benzyne fragmentation (path A). Corresponding vibrational frequencies are listed from the CCSD(T)/cc-pTVZ level of theory.

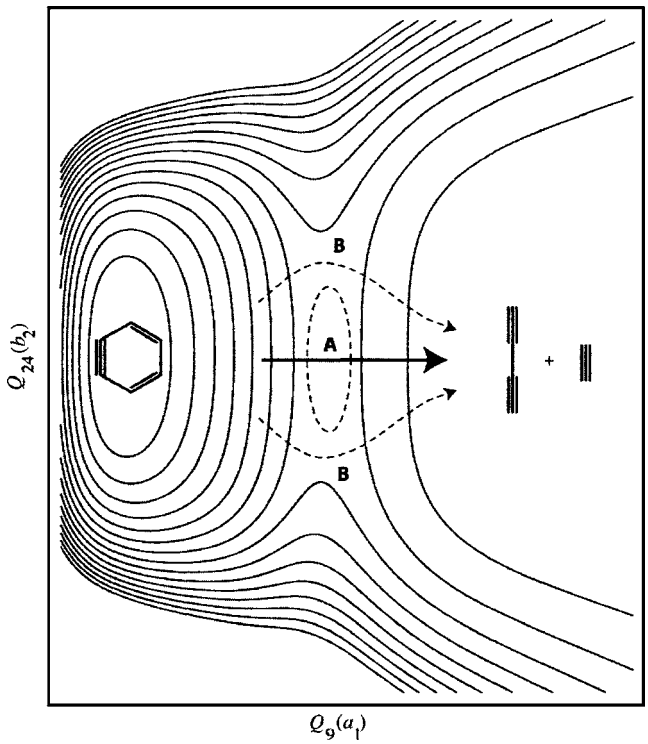

FIG. 14. Schematic energy contours of concerted pathways for *o*-benzyne fragmentation to acetylene+diacetylene. Path A is the classic, concerted retro-Diels-Alder route (C_{2v} symmetry). Shown by dashed lines is a hypothetical path B, which is asymmetric but concerted; it does not pass through a chemical intermediate. The qualitative energy surface is represented in the $Q_9(a_1)$ and $Q_{24}(b_2)$ normal coordinates of the path A transition state, as depicted in Fig. 13.

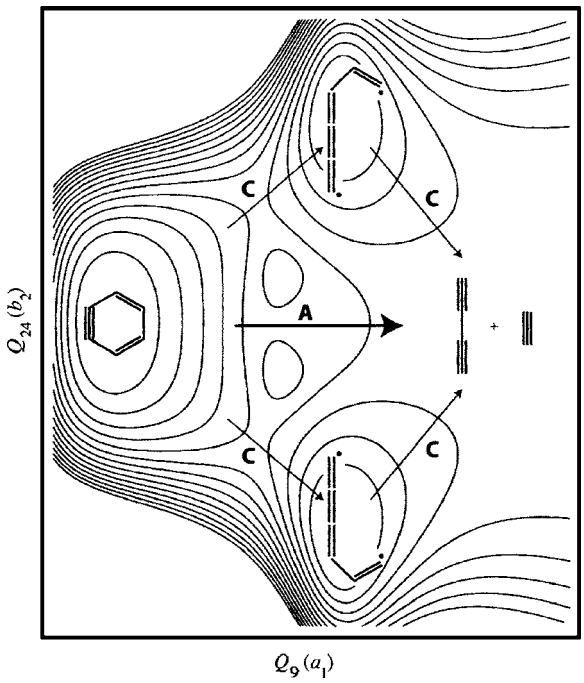

FIG. 15. Schematic energy contours of possible competitive pathways for *o*-benzyne fragmentation to acetylene+diacetylene. Path A is the classic, concerted retro-Diels-Alder route (C_{2v} symmetry). In contrast, path C is an asymmetric, nonconcerted route through an open-chain diradical intermediate. See Fig. 13 and the caption of Fig. 14 for definitions of the $Q_9(a_1)$ and $Q_{24}(b_2)$ geometric coordinates.

lene and diacetylene products cannot be produced by the HCC–CH=CH–CCH intermediate, because the necessary carbon-carbon bond fragmentation must also be accompanied by an unfavorable hydrogen shift. Our preliminary CCSD(T)/cc-pVDZ computations indicated that this process would have to overcome an overall barrier of at least 100 kcal mol^{-1}.

If HCC–CH=CH–CCH is being formed in our experiments, it should be detectable. The *IE*(HCC–CH=CH–CCH) is certainly below 10.487 eV so the 118.2 nm laser line in the PIMS experiment could ionize this species. Likewise the proton affinity or gas-phase acidity of HCC–CH=CH–CCH implies that hex-3-ene-1,5-diyne could react with H_3O^+ or OH^- in the CIMS apparatus. And hex-3-ene-1,5-diyne will have characteristic C–H stretching frequencies for the H–C≡C– and =C–H bonds. The experimental infrared spectra [Figs. 2, 9(a), and 9(b)] are the most persuasive data that indicate the absence of the hex-3-ene-1,5-diyne.

VI. DISCUSSION

A. Mechanisms for high temperature fragmentation of benzene

The decomposition of benzene at high temperatures has been studied in shock tubes.[1,2] From the thermochemistry of Scheme II, it is clear that conditions harsh enough to break the C–H bond in benzene[2] (113 kcal mol^{-1}) can also easily break the remaining C–H bonds to produce any of the isomeric benzynes: *o*-C_6H_4, *m*-C_6H_4, and *p*-C_6H_4. The experiments from this paper (Figs. 1–7) clearly demonstrate that our hyperthermal nozzle generates *o*-C_6H_4. At higher temperatures, the most facile path for *o*-benzyne decomposition is fragmentation to acetylene and diacetylene. Thus we have demonstrated the occurrence of reaction (3). Our study with 3,6-$(CH_3)_2$-*o*-C_6H_2 in Figs. 8, 9(a), and 9(b), demonstrates that at the threshold decomposition temperature, the 3,6-dimethyl-*o*-benzyne does not isomerize but fragments to HCCH and CH_3–CC–CC–CH_3.

We conclude that at high temperatures, the fragmentation path for benzene is exactly that outlined by the reactions (1) → (2) → (3). According to our high-level *ab initio* computations, the concerted, retro-Diels-Alder route (path A) of reaction (3) is completely consistent with the experimental observations. However, there may also be a competitive, nonconcerted route (path C) through an open-chain singlet diradical intermediate, a problem that awaits elucidation by arduous multireference electronic structure studies.

B. Pyrolysis of aromatic fuels

The retro-Diels-Alder cracking of *o*-benzyne may be of greater importance than simply describing the decomposition of benzene. In a shock tube study of the fragmentation of toluene it was discovered that there are two important, parallel reactions.[116] Scheme II indicates that the lowest toluene fragmentation route (90 kcal mol^{-1}) is formation of hydrogen atom and the benzyl radical [Eq. (18a)]. In contrast, C–C

bond scission is higher in energy (104 kcal mol^{-1}) but it produces a pair of polyatomic radicals [Eq. (18b)].

$$C_6H_5CH_3 \rightarrow C_6H_5CH_2 + H, \tag{18a}$$

$$C_6H_5CH_3 \rightarrow C_6H_5 + CH_3. \tag{18b}$$

Scheme II summarizes these enthalpy changes. However, the entropy increase will be more important for Eq. (18b) because it produces a pair of polyatomic radicals. As the temperature increases, the free energy, $\Delta G = \Delta H - T\Delta S$, will increasingly favor Eq. (18b) over Eq. (18a). At some high temperature, the C–C bond cleaving reaction will become the favored decomposition route of toluene: $\Delta_{rxn}G(C_6H_5CH_3 \rightarrow C_6H_5CH_2 + H) > \Delta_{rxn}G(C_6H_5CH_3 \rightarrow C_6H_5 + CH_3)$. The validity of this expectation has been explored using Active Thermochemical Tables (ATcT) resulting in Fig. 16.[117–119]

The pertinent details of ATcT and its underlying thermochemical network approach are given elsewhere.[117] The thermochemical data needed to construct Fig. 16 have been obtained by a statistical analysis and simultaneous solution of the Core (Argonne) Thermochemical Network, C(A)TN, which currently (version 1.052) contains more than 700 chemical species interconnected by roughly 6500 thermochemically relevant experimental and computational determinations, and is growing on a daily basis.[120] The detailed description of the intricacies of C(A)TN is beyond the scope of the present paper. Suffice it to say here that the determinations influencing the ATcT result for the bond dissociation enthalpy of toluene into benzyl and H [reaction (18a)] are those listed in the recent IUPAC recommendation for the thermochemistry of benzyl.[94] The manifold of C(A)TN interdependencies determining the bond dissociation enthalpy of toluene into phenyl and methyl [reaction (18b)] is substantially more complex, but the ATcT sensitivity analysis indicates that the current result is heavily dominated by the negative-ion-cycle determination of the bond dissociation energy of benzene,[21,22] the positive-ion-cycle determinations of the bond dissociation energy of methane,[121–124] and the calorimetric determinations of the combustion enthalpies of methane,[125–132] and liquid benzene[133–135] and toluene,[133,135,136] coupled to the determinations of the vaporization enthalpies of benzene[137–140] and toluene.[137–141] The entropy changes of reactions (18a) and (18b), needed to relate reaction enthalpies to corresponding free energies, and the temperature dependences of the enthalpy and free energy of both reactions are based on the partition functions (and their various derivatives) for toluene, benzyl, phenyl, methyl, and hydrogen atom, contained in ATcT. The partition-function related thermochemical quantities for H are trivially obtained by level counting and are in ATcT the same as in standard thermochemical compilations.[142–145] In the absence of more elaborate information (e.g., full complement of anharmonicities), the partition-function related thermochemical quantities for the other four species were computed internally by ATcT using a rigid-rotor harmonic-oscillator (RRHO) approach, including an explicit treatment of internal rotors (for toluene and benzyl, see discussion in Ref. 94) as implemented by McBride and Gordon in the NASA approach.[146] The spectroscopic constants for toluene,[140,147] phenyl,[17,148] and methyl[149] were taken from the literature, and those for benzyl from the recent IUPAC review.[94]

Though the difference in the enthalpies of reactions (18a) and (18b) is obtained by ATcT quite accurately and reliably at room temperature [based on the thermochemical knowledge content of C(A)TN described above], the accuracy of extrapolation of the relevant thermochemistry to high temperatures is highly dependent on the applicability of the inherently approximate RRHO approach. Nevertheless, the combined ATcT results shown in Fig. 16 are sufficiently accurate to explicitly demonstrate the point that at a sufficiently high temperature $\Delta_{rxn}G(C_6H_5CH_3 \rightarrow C_6H_5CH_2 + H)$ becomes larger than $\Delta_{rxn}G(C_6H_5CH_3 \rightarrow C_6H_5 + CH_3)$. Both the enthalpy (■) and the free energy (●) change for benzyl radical formation, ΔH(18a) and ΔG(18a), are plotted as a function of temperature and compared to the enthalpy (□) and the free energy (°) change for C–C bond scission, ΔH(18b) and ΔG(18b). At roughly 1500 K the free energies of Eqs. (18a) and (18b) become equivalent; $\Delta_{rxn}G(C_6H_5CH_3 \rightarrow C_6H_5CH_2 + H) \cong \Delta_{rxn}G(C_6H_5CH_3 \rightarrow C_6H_5 + CH_3)$.

The kinetics of toluene decomposition[150] follows the thermochemistry of Fig. 16. As predicted earlier,[116] rate constants for fragmentation of a polyatomic molecule to a stable radical [such as $C_6H_5CH_2$ in Eq. (18a)] and a H atom are characterized by *A* factors in the range of 10^{15} s^{-1}, but dissociation to a pair of complex radicals [as in Eq. (18b)] could have *A* factors in excess of 10^{17} s^{-1}. The conclusion of Fig. 16 is that at decomposition temperatures of 1600 K or greater, arenes such as toluene will begin to shed their alkyl groups and produce phenyl radicals. As indicated in Eq. (2) these C_6H_5 radicals will decompose to *o*-C_6H_4 and thence via Eq. (3) to $HC{\equiv}CH + HC{\equiv}C{-}C{\equiv}CH$. Since gasoline contains[151] an appreciable fraction of aromatic hydrocarbons, high engine temperatures may crack these alkylbenzenes to a mixture of alkyl radicals and phenyl radicals. The phenyl radicals will then dissociate first to benzyne and then to acetylene and diacetylene.

ACKNOWLEDGMENTS

The research at the University of Georgia was supported by the U.S. Department of Energy, Office of Basic Energy Sciences, Combustion Program (Grant No. DE-FG02-97ER14748). Experiments at the University of Colorado were supported by grants from the Chemical Physics Program, United States Department of Energy (DE-FG02-87ER13695) and the National Science Foundation (CHE-9813659) to one of the authors (G.B.E.). Two of the authors (V.M.B. and S.K.) thank the National Science Foundation (CHE-0349937) for support. The work at Argonne National Laboratory, together with the underlying fundamental thermochemical development of the ATcT approach, was supported by the U.S. Department of Energy, Division of Chemical Sciences, Geosciences, and Biosciences of the Office of Basic Energy Sciences, under Contract No. W-31-109-ENG-38. Development of inherent computer-science aspects of ATcT and the underpinning data management technologies were supported by the U.S. Department of Energy, Division of Mathematical, Information, and Computa-

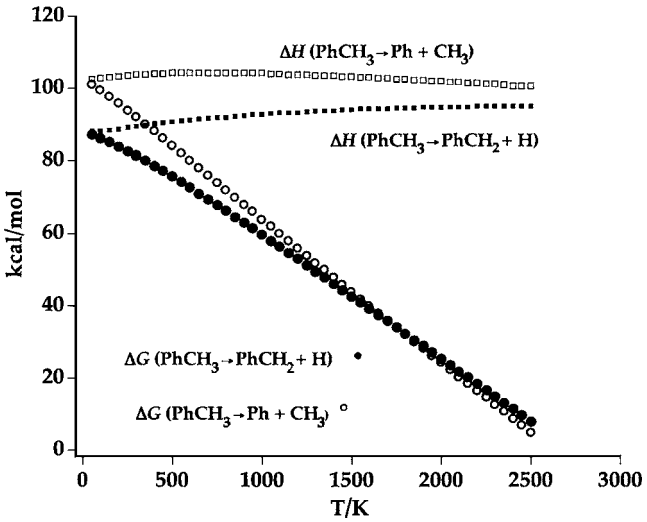

FIG. 16. Variation of the enthalpy of reaction for $\Delta_{rxn}H_T(C_6H_5CH_3 \rightarrow C_6H_5CH_2+H)$ and $\Delta_{rxn}H_T(C_6H_5CH_3 \rightarrow C_6H_5+CH_3)$ as a function of temperature. Both plots are relatively flat out to 2500 K. In contrast the free energies, $\Delta_{rxn}G_T(C_6H_5CH_3 \rightarrow C_6H_5CH_2+H)$ and $\Delta_{rxn}G_T(C_6H_5CH_3 \rightarrow C_6H_5+CH_3)$, both steadily decline. Around 1600 K $\Delta_{rxn}G_T(C_6H_5CH_3 \rightarrow C_6H_5CH_2+H)$ becomes greater than $\Delta_{rxn}G_T(C_6H_5CH_3 \rightarrow C_6H_5+CH_3)$.

tional Science of the Office of Advanced Scientific Computing Research, under Contract Nos. W-31-109-ENG-38 and DE-AC02-06CH11357 (Argonne) as part of the multi-institutional Collaboratory for Multi-Scale Chemical Science (CMCS), which was a project within the National Collaboratories Program of the U.S. Department of Energy. This work has benefited from the support and effort of numerous CMCS Team members. Portions of the research described are related to the effort of a Task Group of the International Union of Pure and Applied Chemistry (2003-024-1-100). The authors thank Dr. Larry B. Harding, Dr. John F. Stanton, and Dr. Alexander Laskin for several enlightening discussions. Barry K. Carpenter spend part of his 2005 sabbatical in Boulder and the authors have benefited a great deal from their conversations with Professor Carpenter. This story about the formation of benzyne from phenyl radicals and its subsequent Diels-Alder fragmentation was first presented by one of the authors (G.B.E.) in January 2006 at Yale University's *Wiberg Lecture*.

[1] S. H. Bauer and C. F. Aten, J. Chem. Phys. **39**, 1253 (1963).
[2] J. H. Kiefer, L. J. Mizerka, M. R. Patel, and H. C. Wei, J. Phys. Chem. **89**, 2013 (1985).
[3] P. R. Westmoreland, A. M. Dean, J. B. Howard, and J. P. Longwell, J. Phys. Chem. **93**, 8171 (1989).
[4] W. Q. Deng, K. L. Han, J. P. Zhan, and G. Z. He, Chem. Phys. Lett. **288**, 33 (1998).
[5] L. V. Moskaleva, L. K. Madden, and M. C. Lin, Phys. Chem. Chem. Phys. **1**, 3967 (1999).
[6] H. Wang, A. Laskin, N. W. Moriarty, and M. Frenklach, Proc. Combust. Inst. **28**, 1545 (2000).
[7] R. R. Jones and R. G. Bergman, J. Am. Chem. Soc. **94**, 660 (1972).
[8] R. G. Bergman, Acc. Chem. Res. **6**, 25 (1973).
[9] J. B. Pedley, R. D. Naylor, and S. P. Kirby, *Thermochemistry of Organic Compounds*, 2nd ed. (Chapman and Hall, New York, 1986).
[10] J. H. Kiefer, S. S. Sidhu, R. D. Kern, K. Xie, H. Chen, and L. B. Harding, Combust. Sci. Technol. **82**, 101 (1992).
[11] S. E. Stein and A. Fahr, J. Phys. Chem. **89**, 3714 (1985).
[12] W. R. Roth, O. Adamczak, R. Breuckmann, H. W. Lennartz, and R. Boese, Chem. Ber. **124**, 2499 (1991).
[13] J. Berkowitz, G. B. Ellison, and D. Gutman, J. Phys. Chem. **98**, 2744 (1994).
[14] S. J. Blanksby and G. B. Ellison, Acc. Chem. Res. **36**, 255 (2003).
[15] P. H. Kasai, E. Hedaya, and P. H. Kasai, J. Am. Chem. Soc. **91**, 4364 (1969).
[16] J. G. Radziszewski, M. R. Nimlos, P. R. Winter, and G. B. Ellison, J. Am. Chem. Soc. **118**, 7400 (1996).
[17] A. V. Friderichsen, J. G. Radziszewski, M. R. Nimlos, P. R. Winter, D. C. Dayton, D. E. David, and G. B. Ellison, J. Am. Chem. Soc. **123**, 1977 (2001).
[18] R. J. McMahon, M. C. McCarthy, C. A. Gottlieb, J. B. Dudek, J. F. Stanton, and P. Thaddeus, Astrophys. J. **590**, L61 (2003).
[19] V. Butcher, M. L. Costa, J. M. Dyke, A. R. Ellis, and A. Morris, Chem. Phys. **115**, 261 (1987).
[20] X. Zhang, Ph.D. thesis, Harvard University, 1995.
[21] R. F. Gunion, M. K. Gilles, M. L. Polak, and W. C. Lineberger, Int. J. Mass. Spectrom. **117**, 601 (1992).
[22] G. E. Davico, V. M. Bierbaum, C. H. DePuy, G. B. Ellison, and R. R. Squires, J. Am. Chem. Soc. **117**, 2590 (1995).
[23] K. M. Ervin and V. F. DeTuri, J. Phys. Chem. A **106**, 9947 (2002).
[24] R. S. Berry, G. N. Spokes, and R. M. Stiles, J. Am. Chem. Soc. **82**, 5240 (1960).
[25] R. S. Berry, G. N. Spokes, and R. M. Stiles, J. Am. Chem. Soc. **84**, 3570 (1962).
[26] R. S. Berry, J. Clardy, and M. E. Schafer, J. Am. Chem. Soc. **86**, 2738 (1964).
[27] R. S. Berry, J. Clardy, and M. E. Schafer, Tetrahedron Lett. **15**, 1003 (1965).
[28] R. S. Berry, J. Clardy, and M. E. Schafer, Tetrahedron Lett. **15**, 1011 (1965).
[29] R. D. Brown, P. D. Godfrey, and M. Rodler, J. Am. Chem. Soc. **108**, 1296 (1986).
[30] S. G. Kukolich, C. Tanjaroom, M. C. McCarthy, and P. Thaddeus, J. Chem. Phys. **119**, 4353 (2003).
[31] S. G. Kukolich, M. C. McCarthy, and P. Thaddeus, J. Phys. Chem. A **108**, 2645 (2004).
[32] X. Zhang and P. Chen, J. Am. Chem. Soc. **114**, 3147 (1992).
[33] W. A. Goddard III, T. H. Dunning, Jr., W. J. Hunt, and P. J. Hay, Acc. Chem. Res. **6**, 368 (1973).
[34] D. G. Leopold, A. E. S. Miller, and W. C. Lineberger, J. Am. Chem. Soc. **108**, 1379 (1986).
[35] J. G. Radziszewski, B. A. Hess, and R. Zahradnik, J. Am. Chem. Soc. **114**, 52 (1992).
[36] Y. L. Guo and J. J. Grabowski, J. Am. Chem. Soc. **113**, 5923 (1991).
[37] J. M. Riveros, S. Ingemann, and N. M. M. Nibbering, J. Am. Chem. Soc. **113**, 1053 (1991).
[38] P. G. Wenthold and R. R. Squires, J. Am. Chem. Soc. **116**, 6401 (1994).
[39] P. G. Wenthold, J. Hu, and R. R. Squires, J. Am. Chem. Soc. **116**, 6961 (1994).
[40] X. Zhang, A. V. Friederichsen, S. Nandi, G. B. Ellison, D. E. David, J. T. McKinnon, T. G. Lindeman, D. C. Dayton, and M. R. Nimlos, Rev. Sci. Instrum. **74**, 3077 (2003).
[41] E. B. Jochnowitz, X. Zhang, M. R. Nimlos, M. E. Varner, J. F. Stanton, and G. B. Ellison, J. Phys. Chem. A **109**, 3812 (2004).
[42] O. L. Chapman, K. Mattes, C. L. McIntosh, J. Pacansky, G. V. Calder, and G. Orr, J. Am. Chem. Soc. **95**, 6134 (1973).
[43] A. L. Brown, D. C. Dayton, M. R. Nimlos, and J. W. Daily, Chemosphere **42**, 663 (2001).
[44] S. Nandi, P. A. Arnold, B. K. Carpenter, M. R. Nimlos, D. C. Dayton, and G. B. Ellison, J. Phys. Chem. A **105**, 7514 (2001).
[45] X. Zhang, V. M. Bierbaum, G. B. Ellison, and S. Kato, J. Chem. Phys. **120**, 3531 (2004).
[46] X. Zhang, S. Kato, V. M. Bierbaum, M. R. Nimlos, and G. B. Ellison, J. Phys. Chem. A **108**, 9733 (2004).
[47] T. H. Dunning, Jr., J. Chem. Phys. **90**, 1007 (1989).
[48] A. K. Wilson, T. van Mourik, and T. H. Dunning, Jr., J. Mol. Struct.: THEOCHEM **388**, 339 (1996).
[49] Extensible Computational Chemistry Environment Basis Set Database, Version 1.0, as developed and distributed by the Molecular Science Computing Facility, Environmental and Molecular Sciences Laboratory, which is part of the Pacific Northwest Laboratory, P.O. Box 999, Richland, Washington 99352, and funded by the U.S. Department of Energy. The Pacific Northwest Laboratory is a multiprogram laboratory operated

by Battelle Memorial Institute for the U.S. Department of Energy under Contract No. DE-AC06-76RLO 1830.
[50] D. E. Woon and T. H. Dunning, Jr., J. Chem. Phys. **103**, 4572 (1995).
[51] C. C. J. Roothaan, Rev. Mod. Phys. **23**, 69 (1951).
[52] W. J. Hehre, L. Radom, P. v. R. Schleyer, and J. A. Pople, *Ab Initio Molecular Orbital Theory* (Wiley-Interscience, New York, 1986).
[53] J. A. Pople and R. K. Nesbet, J. Chem. Phys. **22**, 571 (1954).
[54] A. Szabo and N. S. Ostlund, *Modern Quantum Chemistry: Introduction to Advanced Electronic Structure Theory*, 1st ed., revised (McGraw-Hill, New York, 1989).
[55] B. O. Roos, in *Ab Initio Methods in Quantum Chemistry, Part II*, edited by K. P. Lawley (Wiley, New York, 1987), p. 399.
[56] D. Cremer, in *The Encyclopedia of Computational Chemistry*, edited by P. v. R. Schleyer, N. L. Allinger, T. Clark, J. Gasteiger, P. A. Kollmann, H. F. Schaefer III, and P. R. Schreiner (Wiley, Chichester, 1998), Vol. 3, p. 1706.
[57] T. Helgaker, P. Jørgensen, and J. Olsen, *Molecular Electronic-Structure Theory* (Wiley, Chichester, 2000).
[58] J. A. Pople, J. S. Binkley, and R. Seeger, Int. J. Quantum Chem. **10**, 1 (1976).
[59] R. J. Bartlett, Annu. Rev. Phys. Chem. **32**, 359 (1981).
[60] G. D. Purvis III and R. J. Bartlett, J. Chem. Phys. **76**, 1910 (1982).
[61] J. Paldus, in *New Horizons of Quantum Chemistry*, edited by P.-O. Löwdin and B. Pullmann (Reidel, Dordrecht, 1983), p. 31.
[62] R. J. Bartlett, C. E. Dykstra, and J. Paldus, in *Advanced Theories and Computational Approaches to the Electronic Structure of Molecules*, edited by C. E. Dykstra (Reidel, Dordrecht, 1984), p. 127.
[63] G. E. Scuseria, A. C. Scheiner, T. J. Lee, J. E. Rice, and H. F. Schaefer, J. Chem. Phys. **86**, 2881 (1987).
[64] J. Gauss, in *The Encyclopedia of Computational Chemistry*, edited by P. v. R. Schleyer, N. L. Allinger, T. Clark, J. Gasteiger, P. A. Kollmann, H. F. Schaefer III, and P. R. Schreiner (Wiley, Chichester, 1998), Vol. 1, p. 615.
[65] K. Raghavachari, G. W. Trucks, J. A. Pople, and M. Head-Gordon, Chem. Phys. Lett. **157**, 479 (1989).
[66] G. E. Scuseria and T. J. Lee, J. Chem. Phys. **93**, 5851 (1990).
[67] J. Noga and R. J. Bartlett, J. Chem. Phys. **86**, 7041 (1987).
[68] J. Noga and R. J. Bartlett, J. Chem. Phys. **89**, 3401 (1988).
[69] G. E. Scuseria and H. F. Schaefer III, Chem. Phys. Lett. **152**, 382 (1988).
[70] Y. J. Bomble, J. F. Stanton, M. Kallay, and J. Gauss, J. Chem. Phys. **123**, 054101 (2005).
[71] A. G. Császár, W. D. Allen, and H. F. Schaefer III, J. Chem. Phys. **108**, 9751 (1998).
[72] W. D. Allen, A. L. L. East, and A. G. Császár, in *Structures and Conformations of Non-Rigid Molecules*, edited by J. Laane, M. Dakkouri, B. van der Vecken, and H. Oberhammer (Kluwer, Dordrecht, 1993), p. 343.
[73] A. G. Császár, G. Tarczay, M. L. Leininger, O. L. Polyansky, J. Tennyson, and W. D. Allen, in *Spectroscopy from Space*, edited by J. Demaison and K. Sarka (Kluwer, Dordrecht, 2001), p. 317.
[74] J. M. Gonzales, C. Pak, R. S. Cox, W. D. Allen, H. F. Schaefer, A. G. Császár, and G. Tarczay, Chem.-Eur. J. **9**, 2173 (2003).
[75] M. S. Schuurman, S. R. Muir, W. D. Allen, and H. F. Schaefer III, J. Chem. Phys. **120**, 11586 (2004).
[76] D. Feller, J. Chem. Phys. **98**, 7059 (1993).
[77] T. Helgaker, W. Klopper, H. Koch, and J. Noga, J. Chem. Phys. **106**, 9639 (1997).
[78] Y. Yamaguchi, Y. Osamura, J. D. Goddard, and H. F. Schaefer III, *A New Dimension to Quantum Chemistry: Analytic Derivative Methods in Ab Initio Molecular Electronic Structure Theory* (Oxford University Press, New York, 1994).
[79] J. Gauss, W. J. Lauderdale, J. F. Stanton, J. D. Watts, and R. J. Bartlett, Chem. Phys. Lett. **182**, 207 (1991).
[80] J. D. Watts, J. Gauss, and R. J. Bartlett, J. Chem. Phys. **98**, 8718 (1993).
[81] N. C. Handy, R. D. Amos, J. F. Gaw, J. E. Rice, and E. D. Simandiras, Chem. Phys. Lett. **120**, 151 (1985).
[82] E. D. Simandiras, N. C. Handy, and R. D. Amos, Chem. Phys. Lett. **133**, 324 (1987).
[83] J. Gauss and J. F. Stanton, Chem. Phys. Lett. **276**, 70 (1997).
[84] J. D. Watts, J. Gauss, and R. J. Bartlett, Chem. Phys. Lett. **200**, 1 (1992).
[85] T. J. Lee and A. P. Rendell, J. Chem. Phys. **94**, 6229 (1991).
[86] J. F. Stanton, J. Gauss, J. D. Watts, P. G. Szalay, and R. J. Bartlett with contributions from A. A. Auer, D. B. Bernholdt, O. Christiansen, M. E. Harding, M. Heckert, O. Heun, C. Huber, D. Jonsson, J. Jusélius, W. J. Lauderdale, T. Metzroth, C. Michauk, K. Ruud, F. Schiffmann, and A. Tajti, and the integral packages: MOLECULE (J. Almlöf and P. R. Taylor), PROPS (P. R. Taylor), and ABACUS (T. Helgaker, H. J. Aa. Jensen, P. Jørgensen, and J. Olsen). See also J. F. Stanton, J. Gauss, J. D. Watts, P.. G. Szalay, and R. J. Bartlett, Int. J. Quantum Chem. **26**, 879 (1992). For current version see http://www.aces2.de
[87] H.-J. Werner, P. J. Knowles, M. Schütz *et al.*, MOLPRO, version 2002.6, 2002; http://www.molpro.net
[88] E. Aprà, T. L. Windus, T. P. Straatsma *et al.*, NWCHEM, a computational chemistry package for parallel computers, version 4.7, Pacific Northwest National Laboratory, Richland, Washington, 2005.
[89] R. A. Kendall, E. Apra, D. E. Bernhold *et al.*, Comput. Phys. Commun. **128**, 260 (2000).
[90] M. Kállay and J. Gauss, J. Chem. Phys. **123**, 214105 (2005). The CCSDT(Q) computations were performed with MRCC, a string-based many-body program written by Mihály Kállay.
[91] S. G. Lias, J. E. Bartmess, J. F. Liebman, J. L. Holmes, R. D. Levin, and W. G. Mallard, J. Phys. Chem. Ref. Data Suppl. **17**, 1 (1988). All data taken from the NIST Negative Ion Energetics Database: NIST Standard Reference Database Number 69, June 2005 Release.
[92] K.-C. Lau and C.-Y. Ng, Acc. Chem. Res. **39**, 823 (2006).
[93] B. Ruscic, A. F. Wagner, L. B. Harding *et al.*, J. Phys. Chem. A **106**, 2727 (2002).
[94] B. Ruscic, J. E. Boggs, A. Burcat *et al.*, J. Phys. Chem. Ref. Data **34**, 573 (2005).
[95] Y. Shi and K. M. Ervin, Chem. Phys. Lett. **318**, 149 (2000).
[96] C. E. Moore, *Atomic Energy Levels*, Natl. Bur. Stand. (U.S.) Circ. No. 467 (U.S. GPO, Washington, D.C., 1971.
[97] W. T. Borden, R. J. Loncharich, and K. N. Houk, Annu. Rev. Phys. Chem. **39**, 213 (1988).
[98] K. N. Houk, R. J. Loncharich, J. F. Blake, and W. L. Jorgensen, J. Am. Chem. Soc. **111**, 9172 (1989).
[99] K. N. Houk, Y. Li, and J. D. Evanseck, Angew. Chem., Int. Ed. Engl. **31**, 682 (1992).
[100] H. H. Wenk, M. Winkler, and W. Sander, Angew. Chem., Int. Ed. **42**, 502 (2003).
[101] See EPAPS Document No. E-JCPSA6-126-003702 for a pdf file containing optimum geometric structures of *o*-benzyne, acetylene, diacetylene, and the retro-Diels-Alder transition state at several levels of theory, as well as CCSD(T)/cc-pVDZ harmonic vibrational frequencies for these stationary points. This document can be reached via a direct link in the online article's HTML reference section or via the EPAPS homepage (http://www.aip.org/pubservs/epaps.html).
[102] L. V. Gurvich, I. V. Veyts, C. B. Alcock, and V. S. Iorish, *Thermodynamic Properties of Individual Substances*, 4th ed., Vol. 2, Parts 1 & 2 (Hemisphere, New York, 1991).
[103] J. Gauss and J. F. Stanton, J. Phys. Chem. A **104**, 2865 (2000).
[104] A. C. Scheiner, H. F. Schaefer, and B. Liu, J. Am. Chem. Soc. **111**, 3118 (1989).
[105] T. J. Lee and P. R. Taylor, Int. J. Quantum Chem. **23**, 199 (1989).
[106] P. D. Jarowski, M. D. Wodrich, C. S. Wannere, P. v. R. Schleyer, and K. N. Houk, J. Am. Chem. Soc. **126**, 15036 (2004).
[107] M. Herman, A. Campargue, M. I. El Idrissi, and J. Vander Auwera, J. Phys. Chem. Ref. Data **32**, 921 (2003).
[108] K. L. Bak, J. Gauss, P. Jørgensen, J. Olsen, T. Helgaker, and J. F. Stanton, J. Chem. Phys. **114**, 6548 (2001).
[109] R. B. Woodward and R. Hoffmann, *The Conservation of Orbital Symmetry* (Academic, New York, 1970).
[110] A. M. Mebel, K. Morokuma, and M. C. Lin, J. Chem. Phys. **103**, 3440 (1995).
[111] Of principal concern is the following text from Wang et al. regarding the barrier (critical energy) of the reaction: "Single-point calculations at CASSCF(6,6) MP2/6-31G(*d*) and CASSCF(6,6) MP2/cc-pVTZ yielded a critical energy, E_0, equal to 87 and 72 kcal mol^{-1}, respectively. The enthalpy of reaction of *o*-$C_6H_4 \rightarrow C_2H_2+C_4H_2$ was predicted to be 60 and 44 kcal mol^{-1} with the 6-31G(*d*) and cc-pVTZ basis sets, respectively. These values differ by nearly the same amount as that of the critical energy. Correcting the reaction enthalpies by the thermochemical data of Table I, and assuming that the same correction can be made for the critical energy, we obtained E_0=83 and 84 kcal mol^{-1} with the 6-31G(*d*) and cc-pVTZ basis sets, respectively. These values are supported by a single-point CASPT2/ANO-S calculation, which gave 83 kcal mol^{-1}." According to the data in our Table I, the sensitivity of the reaction energetics to the 6-31G(*d*)→cc-pVTZ basis set improvement should be much less severe than roughly 15 kcal mol^{-1}. In addition, the

CASMP2 method of McDouall et al. employed with the cc-pVTZ basis should not fail so seriously for this problem. [J. J. W. McDouall, K. Peasley, and M. A. Robb, Chem. Phys. Lett. **148**, 183 (1988)].
[112] M. A. Temsamani and M. Herman, J. Chem. Phys. **102**, 6371 (1995).
[113] C. D. Sherrill, E. F. C. Byrd, and M. Head-Gordon, J. Chem. Phys. **113**, 1447 (2000).
[114] M. Allan, J. Chem. Phys. **80**, 6020 (1984).
[115] F. Vila, P. Borowski, and K. D. Jordan, J. Phys. Chem. A **104**, 9009 (2000).
[116] K. M. Pamidimukkala, R. D. Kern, M. R. Patel, H. C. Wei, and J. H. Kiefer, J. Phys. Chem. **91**, 2148 (1987).
[117] B. Ruscic, R. E. Pinzon, M. L. Morton, G. von Laszevski, S. J. Bittner, S. G. Nijsure, K. A. Amin, M. Minkoff, and A. F. Wagner, J. Phys. Chem. A **108**, 9979 (2004).
[118] B. Ruscic, R. E. Pinzon, G. von Laszewski, D. Kodeboyina, A. Burcat, D. Leahy, D. Montoya, and A. F. Wagner, J. Phys.: Conf. Ser. **16**, 561 (2005).
[119] B. Ruscic, *McGraw-Hill Encyclopedia of Science and Technology* (McGraw-Hill, New York, 2004), p. 3.
[120] B. Ruscic, R. E. Pinzon, M. L. Morton, N. K. Srinivasan, M. C. Su, J. W. Sutherland, and J. V. Michael, J. Phys. Chem. A **110**, 6592 (2006).
[121] B. Ruscic, M. Litorja, and R. L. Asher, J. Phys. Chem. A **103**, 8625 (1999).
[122] M. Litorja and B. Ruscic, J. Chem. Phys. **107**, 9852 (1997).
[123] J. A. Blush, P. Chen, R. T. Wiedmann, and M. G. White, J. Chem. Phys. **98**, 3557 (1993).
[124] G. Herzberg, Proc. R. Soc. London, Ser. A **262**, 291 (1961).
[125] F. D. Rossini, J. Res. Natl. Bur. Stand. **6**, 37 (1931).
[126] F. D. Rossini, J. Res. Nat. Bur. Stand. **7**, 329 (1931).
[127] W. A. Roth and H. Banse, Arch. Eisenhuettenwes. **6**, 43 (1932).
[128] F. D. Rossini, Chem. Rev. (Washington, D.C.) **27**, 1 (1940).
[129] D. A. Pittam and G. Pilcher, J. Chem. Soc., Faraday Trans. 1 **68**, 2224 (1972).
[130] A. Dale, C. Lythall, J. Aucott, and C. Sayer, Thermochim. Acta **382**, 47 (2002).
[131] Y. I. Alexsandrov, E. N. Korchagina, and A. G. Chunovkina, Meas. Tech. **45**, 268 (2002).
[132] Y. I. Alexandrov, Thermochim. Acta **382**, 55 (2002).
[133] E. J. Prosen, R. Gilmont, and F. D. Rossini, J. Res. Natl. Bur. Stand. **34**, 65 (1945).
[134] W. H. Johnson, E. J. Prosen, and F. D. Rossini, J. Res. Natl. Bur. Stand. **39**, 49 (1947).
[135] W. D. Good and N. K. Smith, J. Chem. Eng. Data **14**, 102 (1969).
[136] J. Coops, D. Mulder, J. W. Dienske, and J. Smittenberg, Rev. Trav. Chim. **65**, 128 (1946).
[137] V. Majer and V. Svoboda, *Enthalpies of Vaporization of Organic Compounds: A Critical Review and Data Compilation* (Blackwell, Oxford, 1985).
[138] N. S. Osborne and D. C. Ginnings, J. Res. Natl. Bur. Stand. **39**, 453 (1947).
[139] N. L. Yarym-Agaev, N. N. Feodosev, and K. G. Skorikov, Zh. Oxford. Fiz. Khim. **24**, 1061 (1950).
[140] R. J. L. Andon, J. D. Cox, E. F. G. Herington, and J. F. Martin, Trans. Faraday Soc. **53**, 1074 (1957).
[141] D. W. Scott, G. B. Guthrie, J. F. Messerly, S. S. Todd, W. T. Berg, I. A. Hossenlopp, and J. P. McCullough, J. Phys. Chem. **66**, 911 (1962).
[142] J. D. Cox, D. D. Wagman, and V. A. Medvedev, *CODATA Key Values for Thermodynamics* (Hemisphere, New York, 1989).
[143] L. V. Gurvich, I. V. Veyts, and C. B. Alcock, *Thermodynamic Properties of Individual Substances*, 4th ed., Vol. 1, Parts 1 & 2 (Hemisphere, New York, 1989).
[144] M. W. Chase, Jr., C. A. Davies, J. R. Downey, Jr., D. J. Frurip, R. A. McDonald, and A. N. Syverud, Thermochemical Tables, 3rd ed., J. Phys. Chem. Ref. Data Suppl. **14**, 1 (1985).
[145] M. W. Chase, Jr., NIST-JANAF Thermochemical Tables, 4th ed., J. Phys. Chem. Ref. Data Monogr.9 (1998).
[146] B. J. McBride and S. Gordon, *Properties and Coefficients: Computer Program for Calculating and Fitting Thermodynamic Functions*, NASA Ref. Pub. 1271 (NASA, Cleveland, 1992).
[147] A. P. Hitchcock and J. D. Laposa, J. Mol. Spectrosc. **54**, 223 (1975).
[148] M. E. Jacox, J. Phys. Chem. Ref. Data **32**, 1 (2003).
[149] M. E. Jacox, J. Phys. Chem. Ref. Data Monogr.3 (1994).
[150] S. J. Klippenstein, L. B. Harding, and Y. Georgievskii, Appl. Categ. Struct. (submitted).
[151] T. L. Conner, W. A. Lonneman, and R. L. Seila, J. Air Waste Manage. Assoc. **45**, 383 (1995).

Table S1. Optimum geometric structures (Å or deg) of *o*-benzyne at various levels of theory[a]

	r_1	r_2	r_3	r_4	r_5	r_6	θ_1	θ_2	θ_3	θ_4	θ_5
HF / cc-pVDZ	1.4119	1.3942	1.3866	1.2272	1.0833	1.0798	122.60	109.93	127.47	118.45	127.19
HF / cc-pVTZ	1.4075	1.3877	1.3807	1.2160	1.0744	1.0704	122.54	109.88	127.58	118.45	127.18
MP2 / cc-pVDZ	1.4197	1.4165	1.4008	1.2801	1.0965	1.0940	122.73	110.64	126.63	118.72	126.94
MP2 / cc-pVTZ	1.4071	1.4055	1.3866	1.2622	1.0828	1.0798	122.68	110.48	126.84	118.75	127.04
CCSD / cc-pVDZ	1.4221	1.4150	1.4019	1.2670	1.0968	1.0939	122.53	110.73	126.74	118.63	126.69
CCSD / cc-pVTZ	1.4092	1.4019	1.3871	1.2472	1.0819	1.0786	122.51	110.52	126.98	118.63	126.83
CCSD(T) / cc-pVDZ	1.4235	1.4218	1.4055	1.2800	1.0987	1.0959	122.48	111.06	126.46	118.75	126.48
CCSD(T) / cc-pVTZ	1.4106	1.4093	1.3906	1.2603	1.0840	1.0808	122.47	110.80	126.73	118.75	126.66
c~CCSD(T)-AE / cc-pCVQZ	1.4048	1.4035	1.3846	1.2539	1.0819	1.0788	122.46	110.78	126.76	118.77	126.72

[a] See text figures for coordinate labels.

Table S2. Optimum geometric structures (Å or deg) of the (C_{2v}) retro-Diels Alder transition state for *o*-benzyne fragmentation at various levels of theory[a]

	r_1	r_2	r_3	r_4	r_5	r_6	θ_1	θ_2	θ_3	θ_4	θ_5
HF / cc-pVDZ	1.2342	2.1487	1.2346	1.3324	1.0679	1.0684	117.98	101.06	140.96	149.28	152.89
HF / cc-pVTZ	1.2246	2.1325	1.2241	1.3220	1.0583	1.0582	118.03	100.82	141.15	148.67	153.22
MP2 / cc-pVDZ	1.2640	2.2209	1.2718	1.3507	1.0797	1.0830	117.81	100.88	141.32	152.62	151.68
MP2 / cc-pVTZ	1.2475	2.2046	1.2538	1.3334	1.0655	1.0680	117.90	100.06	142.04	152.70	153.00
CCSD / cc-pVDZ	1.2589	2.1972	1.2630	1.3556	1.0814	1.0832	117.86	101.36	140.78	150.78	151.69
CCSD / cc-pVTZ	1.2411	2.1712	1.2437	1.3370	1.0658	1.0669	117.95	100.83	141.23	150.63	152.76
CCSD(T) / cc-pVDZ	1.2643	2.2327	1.2712	1.3594	1.0831	1.0854	117.69	101.17	141.14	151.64	151.22
CCSD(T) / cc-pVTZ	1.2466	2.2068	1.2518	1.3410	1.0676	1.0692	117.81	100.51	141.69	151.67	152.59
c~CCSD(T)-AE / cc-pCVQZ	1.2409	2.1975	1.2457	1.3350	1.0659	1.0673	117.84	100.35	141.81	151.50	152.98

[a] See text figures for coordinate labels.

Table S3. Optimum geometric structures (Å) of acetylene and diacetylene at various levels of theory[a]

	Diacetylene			Acetylene	
	r_1	r_2	r_3	r_1	r_2
HF / cc-pVDZ	1.0637	1.1936	1.3920	1.0639	1.1918
HF / cc-pVTZ	1.0538	1.1822	1.3850	1.0540	1.1801
MP2 / cc-pVDZ	1.0762	1.2372	1.3842	1.0755	1.2297
MP2 / cc-pVTZ	1.0620	1.2194	1.3687	1.0615	1.2114
CCSD / cc-pVDZ	1.0777	1.2258	1.3984	1.0776	1.2228
CCSD / cc-pVTZ	1.0620	1.2067	1.3821	1.0620	1.2033
CCSD(T) / cc-pVDZ	1.0793	1.2336	1.3953	1.0790	1.2287
CCSD(T) / cc-pVTZ	1.0639	1.2150	1.3789	1.0637	1.2097
c~CCSD(T)-AE / cc-pCVQZ	1.0620	1.2093	1.3741	1.0620	1.2038
CCSD(T)-AE / cc-pCVQZ	1.0621	1.2091	1.3742	1.0621	1.2037

[a] See text figures for coordinate labels.

Table S4. CCSD(T)/cc-pVDZ vibrational frequencies along the retro-Diels-Alder fragmentation path of *o*-benzyne

mode	*o*-benzyne	transition state	products
$\omega_1(a_1)$	3220	3412	3500 (σ_g C_2H_2)
$\omega_2(a_1)$	3195	3369	3454 (σ_g C_4H_2)
$\omega_3(a_1)$	1881	1995	2215 (σ_g C_4H_2)
$\omega_4(a_1)$	1474	1742	1986 (σ_g C_2H_2)
$\omega_5(a_1)$	1324	1106	885 (σ_g C_4H_2)
$\omega_6(a_1)$	1147	832	734 (π_u C_2H_2)
$\omega_7(a_1)$	1054	686	584 (π_u C_4H_2)
$\omega_8(a_1)$	995	391	220 (π_u C_4H_2)
$\omega_9(a_1)$	599	615*i*	0
$\omega_{10}(a_2)$	925	595	598 (π_g C_4H_2)
$\omega_{11}(a_2)$	848	553	527 (π_g C_2H_2)
$\omega_{12}(a_2)$	551	447	453 (π_g C_4H_2)
$\omega_{13}(a_2)$	413	245	0
$\omega_{14}(b_1)$	896	650	734 (π_u C_2H_2)
$\omega_{15}(b_1)$	734	597	584 (π_u C_4H_2)
$\omega_{16}(b_1)$	379	218	220 (π_u C_4H_2)
$\omega_{17}(b_2)$	3217	3370	3455 (σ_u C_4H_2)
$\omega_{18}(b_2)$	3178	3353	3410 (σ_u C_2H_2)
$\omega_{19}(b_2)$	1494	1833	2034 (σ_u C_4H_2)
$\omega_{20}(b_2)$	1411	813	598 (π_g C_4H_2)
$\omega_{21}(b_2)$	1249	710	527 (π_g C_2H_2)
$\omega_{22}(b_2)$	1101	466	0
$\omega_{23}(b_2)$	840	414	453 (π_g C_4H_2)
$\omega_{24}(b_2)$	455	93*i*	0